# Functional Assessment of Single Nucleotide Polymorphisms in Nir2 in the Context of Neurodegeneration

*Master's Thesis submitted to the Indian Institute of Science Education and Research Pune in partial fulfilment of the requirements for the BS-MS Dual Degree Programme*


By

**Ashli Jain**
(Reg. No. 20191082)


**Indian Institute of Science Education and Research Pune**
Dr. Homi Bhabha Road, Pashan, Pune 411008, INDIA.

Under the supervision of **Prof. Raghu Padinjat**
at **National Centre for Biological Sciences (NCBS)**


March 2024

## Certificate

This is to certify that this dissertation entitled “Functional Assessment of Single Nucleotide Polymorphisms in Nir2 in the Context of Neurodegeneration” is submitted towards the partial fulfilment of the BS-MS dual degree programme at the Indian Institute of Science Education and Research, Pune represents study/work carried out by Ashli Jain at the National Centre for Biological Sciences under the supervision of Prof. Raghu Padinjat, during the academic year 2023-24.

Ashli Jain

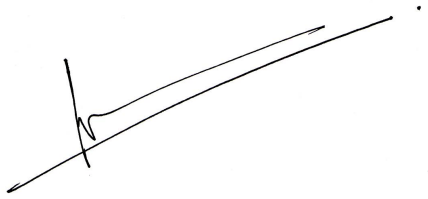

Prof. Raghu Padinjat

This Thesis is Dedicated to

Smt. Puran Devi Goel

## Declaration

I hereby declare that the matter embodied in the report entitled “Functional Assessment of Single Nucleotide Polymorphisms in Nir2 in the Context of Neurodegeneration” are the results of the work carried out by me at the National Centre for Biological Sciences, under the supervision of Prof. Raghu Padinjat and the same has not been submitted elsewhere for any other degree. Wherever others contribute, every effort is made to indicate this clearly, with due reference to the literature and acknowledgement of collaborative research and discussions.

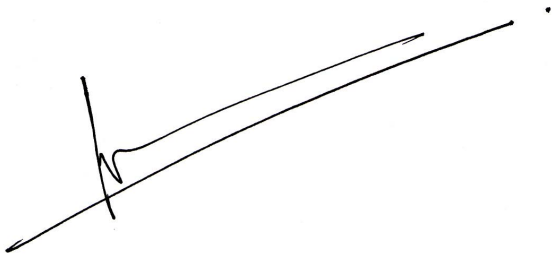

Ashli Jain

Registration Number: 20191082

Prof. Raghu Padinjat

## Table of Contents


Certificate …… 1

Declaration …….. 3

Table of Contents ……... 4

List of Figures ……. 5

List of Tables ……... 6

List of Abbreviations …….. 7

Acknowledgments ……... 8

Abstract …….. …… 9

Contributions …….. 10

CHAPTER I: INTRODUCTION …… 11

CHAPTER II: AIM AND OBJECTIVES ……... 21

CHAPTER III: MATERIALS AND METHODS …… 22

CHAPTER IV: RESULTS …….. 31

CHAPTER V: DISCUSSION ……..... 52

References …….. 55

## List of Figures

**Figure 1:** Classification of PITPs ……...…… 13

**Figure 2:** Lipid transfer function of Nir2 ……...……. 15

**Figure 3:** Role of Nir2 in regulating $PIP_2$ signalling …… 16

**Figure 4:** Intracellular $Ca^{2+}$ release downstream of $PIP_2$ hydrolysis ……. 17

**Figure 5:** Effects of Nir2 depletion …….…… 20

**Figure 6:** $Ca^{2+}$ Imaging experiment protocol …… 28

**Figure 7:** SNPs in the *PITPNM1* gene …….. 31

**Figure 8:** Multiple sequence alignment of Nir2 homologues …….. 32

**Figure 9:** Multiple sequence alignment of PITP domain-containing proteins .. 33

**Figure 10:** Structural alignment of the protein-membrane complex ……. 37

**Figure 11:** RMSD, RMSF and Minimum-Distance plots …… 39

**Figure 12:** Verification of fragments for Gibson assembly …… 40

**Figure 13:** Colony PCR …… 41

**Figure 14:** Construct verification by transfection …… 42

**Figure 15:** Verification of successful incorporation of SNPs …….. 42

**Figure 16:** Comparison of protein localisation at basal state ……... 43

**Figure 17:** Comparison of protein localisation following PLC activation …….. 44

**Figure 18:** Comparison of protein expression …….. 45

**Figure 19:** $[Ca^{2+}]_i$ in Control and Nir2 depleted HEK-M1 cells ……... 47

**Figure 20:** Selection of HEK-M1 cells to be used for analysis …….. 48

**Figure 21:** Rescue of decreased $[Ca^{2+}]_i$ of Nir2 depleted HEK-M1 cells …….. 49

**Figure 22:** $[Ca^{2+}]_i$ in Nir2 variant HEK-M1 cells …… 50

**Figure 23:** RDGB Protein annotated with PI binding residues …….. 54

## List of Tables

**Table 1:** SIFT and Polyphen-2 predictions ..... 34

**Table 2:** Sequence alignment results of Nir2 and RDGB ..... 35

**Table 3:** Corresponding amino acid substitutions in RDGB ..... 35

**Table 4:** FoldX Predictions ..... 36

## List of Abbreviations

| | |
|---|---|
| SCA | Spinocerebellar ataxia |
| SNP | Single nucleotide polymorphism |
| ER | Endoplasmic reticulum |
| PM | Plasma membrane |
| PI | Phosphatidylinositol |
| PA | Phosphatidic acid |
| PLC | Phospholipase C |
| $PIP_2$ | Phosphatidylinositol 4,5-bisphosphate |
| LTP | Lipid transfer protein |
| PITP | Phosphatidylinositol transfer protein |
| PITPd | PITP domain |
| GPCR | G protein-coupled receptor |
| $IP_3$ | Inositol trisphosphate |
| DAG | Diacylglycerol |
| mGluR1 | Metabotropic glutamate receptor Type 1 |
| TRPC3 | Transient receptor potential channel C3 |
| PKC | Protein kinase C |
| MDS | Molecular Dynamics Simulation |
| DPPC | Dipalmitoylphosphatidylcholine |

## Acknowledgements

First and foremost, I express my sincere gratitude to Prof. Raghu Padinjat for entrusting me with the opportunity to embark on this remarkable project and for his unwavering guidance throughout its development. I am indebted to Dr Sankhanil Saha and Dr Harini Krishnan for their invaluable mentorship and constant support at every juncture of my journey.

I thank all current and past members of the Flyfat Lab whose foundational work laid the groundwork for this project. Their guidance and encouragement have been indispensable and have kept me motivated throughout. Additionally, I extend my thanks to the Central Imaging & Flow Cytometry Facility, the Sequencing Facility, the Instrumentation Department, and the Lab Kitchen for their resources and contributions.

I am also grateful to my internal expert, Prof. Thomas Pucadyil, for his insightful inputs and support. Furthermore, I extend my thanks to IISER Pune for providing me with vital resources and the environment that have facilitated this research endeavour.

No words can adequately express my gratitude to my dear friend Likhith Chandragiri, whose support has been instrumental in the completion of my MS thesis, and my friends who have stood by me throughout this journey. Their encouragement and camaraderie have meant the world to me.

Finally, and most importantly, I am thankful to my family for their unyielding support- my father, Piyush Jain, my mother, Shalini Jain, and my sister, Navya Jain. Their love and encouragement have been my pillars of strength.

## Abstract

Nir2 is a lipid transfer protein that operates at the endoplasmic reticulum (ER) - plasma membrane (PM) contact sites, facilitating the transfer of phosphatidylinositol (PI) from ER to PM and phosphatidic acid (PA) in the opposite direction. This process plays a crucial role in maintaining phospholipase C (PLC)-dependent Phosphatidylinositol 4,5-bisphosphate ($PIP_2$) signalling.

Whole exome sequencing data from a cohort of patients with clinical features like cerebellar dysfunction, suggestive of Spinocerebellar Ataxia (SCA), revealed Single Nucleotide Polymorphisms (SNPs) in the Nir2-encoding *PITPNM1* gene in six patients. Two of these SNPs (K191E and Q135P) were found in the PITP domain of Nir2.

We hypothesise that SNPs in this domain might cause aberrant PI-transfer function of the protein, consequently disrupting $PIP_2$ signalling and thereby perturbing the downstream $Ca^{2+}$ homeostasis. Previous studies show evidence that dysregulated $Ca^{2+}$ homeostasis could contribute to the onset and progression of several neurodegenerative disorders, including SCA.

Molecular dynamics simulation predicted that only one of the SNPs (K191E) adversely affected the structure, stability, and function of Nir2. Experimental validation revealed no alterations in the expression and localisation of Nir2 containing either of the SNPs (K191E and Q135P). However, assessment of receptor-activated intracellular $Ca^{2+}$ release as a readout of Nir2 function demonstrated significant functional impairment.

## Contributions

| Contributor Role | Contributor Name |
|---|---|
| Conceptualisation Ideas | Prof Raghu Padinjat, Ashli Jain, Dr Sankhanil Saha, Dr Harini Krishnan, |
| Methodology | Ashli Jain, Dr Sankhanil Saha, Dr Harini Krishnan, |
| Software | - |
| Validation | Ashli Jain, Dr Sankhanil Saha, Dr Harini Krishnan |
| Formal analysis | Ashli Jain |
| Investigation | Ashli Jain, Dr Sankhanil Saha, Dr Harini Krishnan, Vaisaly R. Nath, Thejaswini BG |
| Resources | Prof Raghu Padinjat, Dr Sankhanil Saha, Dr Harini Krishnan |
| Data Curation | Ashli Jain, Dr Sankhanil Saha, Dr Harini Krishnan |
| Writing - Original draft preparation | Ashli Jain |
| Writing - Review and editing | Prof Raghu Padinjat, Dr Sankhanil Saha, Dr Harini Krishnan, Ashli Jain |
| Visualisation of Results | Ashli Jain |
| Supervision | Prof Raghu Padinjat, Dr Sankhanil Saha, Dr Harini Krishnan |
| Project administration | Prof Raghu Padinjat |
| Funding acquisition | Prof Raghu Padinjat |

*The contributor syntax is based on the Journal of Cell Science CRediT Taxonomy.

# CHAPTER I: INTRODUCTION

## Spinocerebellar Ataxia: A Neurodegenerative Disorder

Ataxia, translating to 'absence of order,' is a disorder characterised by uncoordinated voluntary movements, often stemming from cerebellar dysfunction. It is a symptom of an underlying condition and not a clinical disorder on its own. Ataxia can arise from a range of causes, spanning both genetic and non-genetic origins. Among the genetic causes, spinocerebellar ataxias (SCAs) constitute a significant subset (Ashizawa & Xia, 2016).

The SCAs comprise a genetically diverse set of autosomal dominantly inherited disorders. Owing to their heterogeneity, currently, there are 42 known genetically distinct subtypes of SCAs. Their defining clinical characteristic is a gradual deterioration in balance and coordination, often accompanied by speech difficulties. (Klockgether *et al.*, 2019).

From a genetic standpoint, SCAs can be broadly categorised into two groups: those resulting from dynamic repeat expansion within DNA sequences and those stemming from non-repeat mutations such as missense mutations, nonsense mutations, insertions, or deletions. SCA typically emerges during mid-adulthood, although it can also appear in childhood or old age, encompassing a wide range of ages for onset. This condition significantly limits the mobility and communication abilities of affected individuals, greatly impacting their quality of life (QOL). Moreover, many SCAs can result in premature death among patients (Durr A., 2010; Klockgether *et al.*, 2019).

## SNPs in the *PITPNM1* Gene

Whole exome sequencing of a cohort of adult patients with clinical features indicative of cerebellar dysfunction, as seen in several SCAs, was carried out by Dr. Marcello Scala at the University of Genoa, Italy. Sequence analysis revealed that seven patients from the cohort had Single Nucleotide Polymorphisms (SNPs) in the *PITPNM1* gene.

Single Nucleotide Polymorphism i.e. change in a single nucleotide position can be synonymous (i.e. it does not change encoded amino acids) or nonsynonymous (i.e. it changes encoded amino acids). Nonsynonymous SNPs in genes can affect the promoter activity or pre-mRNA conformation, thereby altering the translated protein's ability to bind to its substrate or inhibitors. They can also affect the protein's expression levels and subcellular localisation, rendering it non-functional (Shastry B. S., 2007).

Six of the seven SNPs in the *PITPNM1* gene, found in the patients under study were non-synonymous in nature, sparking an interest to uncover whether these specific SNPs in the *PITPNM1* gene had a role to play in the onset and progression of their neurodegenerative symptoms. The *PITPNM1* gene in mammals encodes for Nir2, which belongs to a specific class of lipid transfer protein (LTP) that can bind and transfer phosphatidylinositol.

LTPs are a special class of proteins that greatly facilitate monomeric lipid exchange between membranes by placing the lipids in their hydrophobic pocket and shuttling them through an aqueous environment. Consequently, LTPs can locally alter the lipid composition of membranes, thereby regulating diverse cellular functions such as vesicular trafficking, signal transduction, and lipid metabolism (Lev S., 2010).

LTPs have further been divided into 27 distinct protein families across various organisms based on their sequence, structural similarity, and ability to transport specific lipid classes (Raghu *et al.*, 2021).

## The PITP Class of Proteins

PITPs, or Phosphatidylinositol transfer proteins, are a class of LTPs that can transfer phosphatidylinositol (PI) between membranes. Members of this class of proteins are identified by the presence of an N-terminal PITP domain (PITPd). Based on the similarity in sequence of this PITPd, PITPs are further divided into the following sub-classes (***Figure 1***): Class I PITPs include PITPα and PITPβ, each possessing a

single PITPd. Class II comprises (i) Class IIA PITPs (also known as “multi-domain” PITPs), containing additional motifs and domains alongside the PITPd, and (ii) Class IIB PITPs that contain a short tail of amino acids, C-terminal to the PITPd. Despite both classes being capable of PI transfer, Class I PITPs can additionally transfer Phosphatidylcholine (PC), whereas Class II PITPs can transfer Phosphatidic Acid (PA) (Raghu *et al.*, 2021; Cockcroft & Carvou, 2007).

The Retinal Degeneration B (RDGB) protein found in Drosophila is the founding member of the multidomain Class II PITPs. As a result, this group is also known as the “RDGB family of proteins”. Its name originates from the fact that mutations in the gene that encodes for RDGB (*rdgB*) lead to the degeneration of photoreceptors in the retina (Trivedi & Padinjat, 2007). The Nir proteins (Nir2 and Nir3 in humans) are mammalian homologues of the RDGB protein. Since they can interact with the “N-terminal domain of protein tyrosine kinase PYK-2”, they are called Nir (N-terminal domain-interacting receptors) proteins. They belong to Class IIA PITPs and, thus, have an N-terminal PITP domain, an FFAT motif and the C-terminal domains, the DDHD domain and the LNS2 domain (***Figure 1***) (Lev *et al.*, 1999; Hsuan & Cockcroft, 2001).

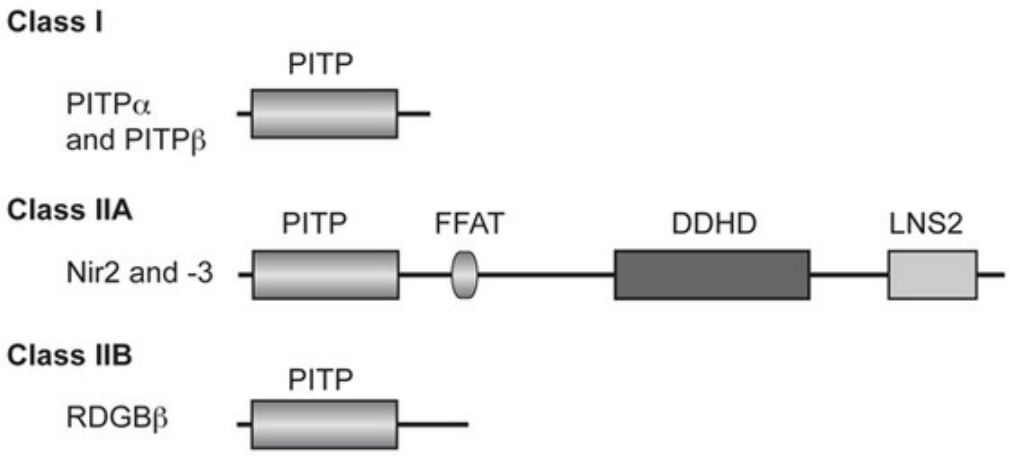


***Figure 1: Classification of PITPs (Kim et al., 2016; Hsuan & Cockcroft, 2001)***
*PITPs can be divided into two subgroups: Class I and Class II. Nir2 is a Class IIA PITP, which is characterised by the presence of an N-terminal PITP domain, an FFAT motif and C-terminal DDHD and LNS2 domains.*

The PITP domain is chiefly concerned with binding and transferring lipids. Though there is limited information about the structure of the PITPd of Class II PITPs, PITPd of Class I PITPs are known to possess a “lipid-binding core”, a “regulatory loop”, and the “C-terminal region” (Raghu *et al*., 2021).

The FFAT (diphenylalanine (FF) in an acidic tract) motif is a short peptide sequence containing the “EFFDAxE" amino acid sequence, which functions as an ER targeting signal. The interaction of Nir2 and VAP (which is an ER resident protein) is mediated by the FFAT motif, which plays a vital role in the protein’s localisation (Peretti *et al*., 2008; Amarilio *et al.*, 2005; Slee & Levine, 2019).

There is also a large unstructured region located between the FFAT motif and the DDHD domain, which has been demonstrated to be crucial for the interaction between RDGB and VAP (Basak *et al.*, 2021).

The DDHD domain gets its name from the four conserved amino acids D, D, H and D, present, which are predicted to constitute a site for binding divalent metals. Recent studies have shown that mutations in these conserved residues lead to localisation defects and loss of RDGB function *in vivo*. Additionally, it has been shown that physical interaction between the DDHD domain and the LNS2 domain influences the localisation of the protein (Basak *et al.*, 2021). The LNS2 domain has been shown to bind to PA and facilitate the localisation of the protein to the plasma membrane (PM) *in vitro* (Kim *et al*., 2013; Basak *et al.*, 2021).

## Nir2: A Regulator of Phosphatidylinositol 4,5-bisphosphate ($PIP_2$) Signalling

Nir2 is a multidomain, Class IIA PITP that can transfer Phosphatidylinositol (PI) from ER to PM and Phosphatidic Acid (PA) in the opposite direction (***Figure 2***). This transfer occurs when Nir2 is localised to the ER-PM contact sites, which are locations where sub-cellular membranes are placed in close proximity (10-30 nm) (Kim *et al*., 2015; Krishnan *et al.*, 2023).

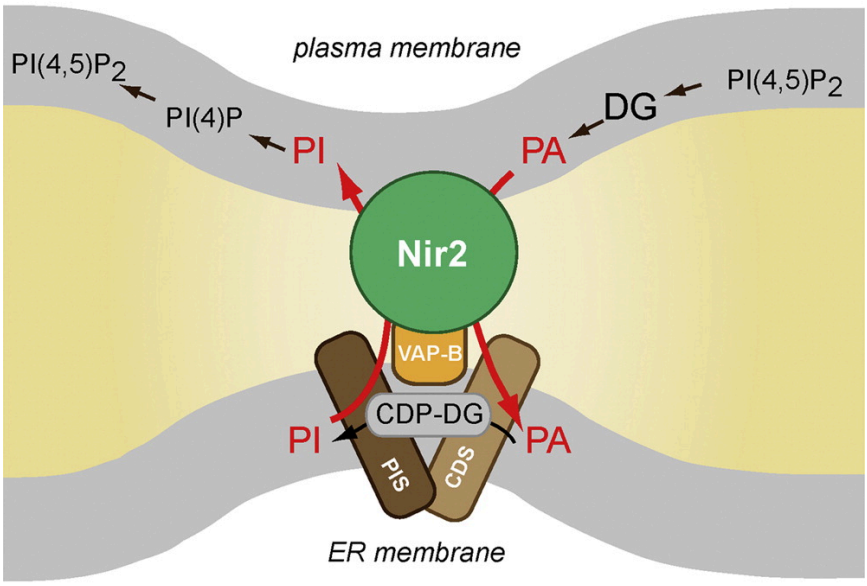


***Figure 2: Nir2 transfers lipids at the ER-PM contact sites (Kim et al., 2015)***
*Nir2 transports PI from ER to PM and PA from PM to ER. The transfer occurs at the ER-PM contact sites.*

PI is the precursor of Phosphatidylinositol 4,5-bisphosphate ($PIP_2$), which is a low abundance membrane lipid that is involved in a number of key cellular events like membrane trafficking, PM-cytoskeleton linkages, etc. Downstream of agonist-mediated GPCR signalling, Phospholipase C (PLC) is activated, which results in the hydrolysis of $PIP_2$, generating two secondary messengers: inositol 1,4,5-trisphosphate ($IP_3$) and diacylglycerol (DAG). This, in turn, leads to the $PIP_2$ pool getting depleted at the PM (***Figure 3***) (Balla T., 2013; Berridge, 1984)

For a subsequent bout of PLC-mediated signalling, it is necessary to re-synthesise $PIP_2$ from its precursor PI, which is primarily synthesised within the ER. Furthermore, it is important to translocate PA (formed by the phosphorylation of DAG at the PM) to the ER for subsequent enzymatic conversion into PI (***Figure 3***) (Bill & Vines, 2020; Cockcroft & Padinjat, 2016).

Thus, PI/PA transfer by Nir2 is essential to maintain the $PIP_2$ pool at the PM and thereby regulating the $PIP_2$ signalling.

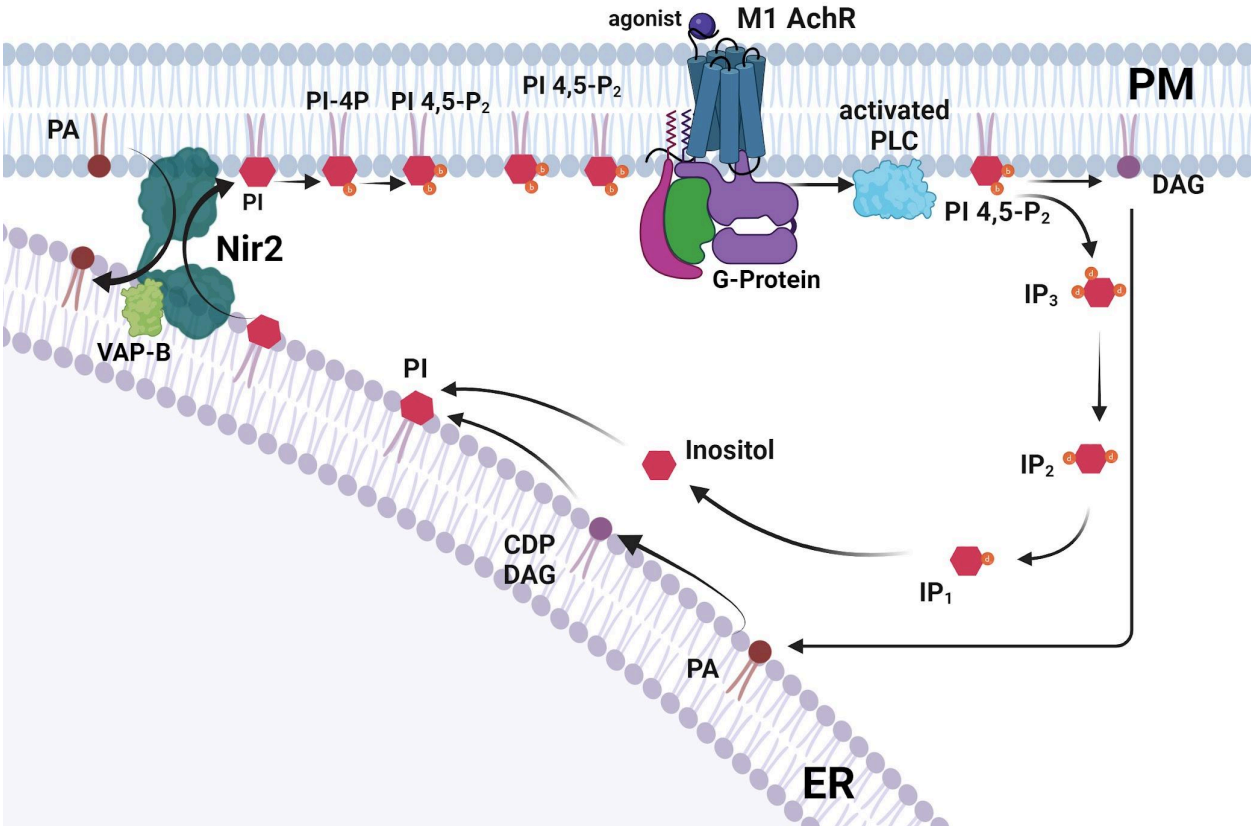


***Figure 3: Role of Nir2 in regulating $PIP_2$ signalling (Saha et al., 2023)***

$IP_3$, one of the secondary messengers generated upon $PIP_2$ hydrolysis, is a small water-soluble molecule that binds to the $IP_3$ receptor channels on the ER. This facilitates the release of $Ca^{2+}$ from the ER stores, resulting in a rise in intracellular $Ca^{2+}$ (***Figure 4***) (Prole & Taylor, 2019).

Replenishment of $Ca^{2+}$ in the ER stores occurs through a mechanism called store-operated calcium entry (SOCE), wherein $Ca^{2+}$ rushes into the cytoplasm from the extracellular medium through specialised channels, subsequently diffusing into the ER (Prakriya & Lewis, 2015).

Thus, perturbations in the Nir2 function can affect not only the resynthesis of $PIP_2$ at the PM and, thereby, the downstream signalling but also the $Ca^{2+}$ homeostasis in cells.

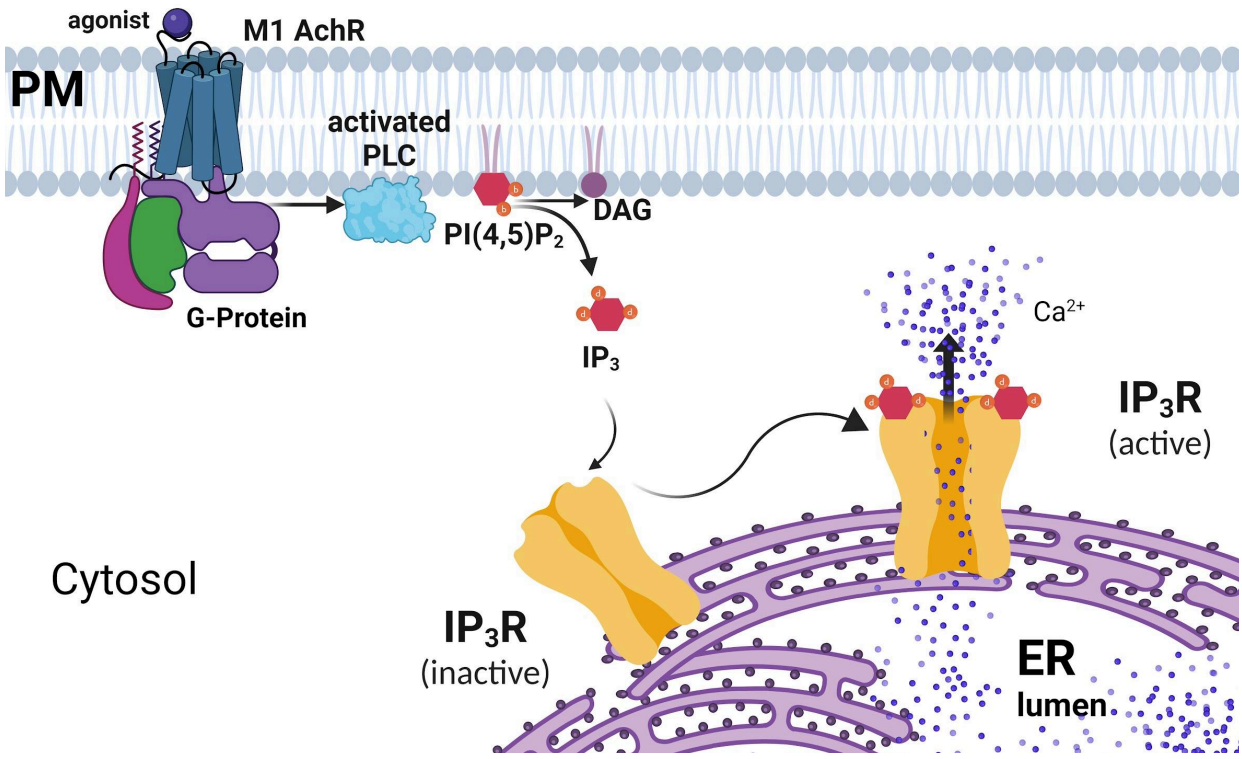


***Figure 4: Intracellular $Ca^{2+}$ release downstream of $PIP_2$ hydrolysis (Sankhanil's PhD Thesis, 2023)***

## Calcium Homeostasis and Neurodegeneration

$Ca^{2+}$ plays a pivotal role as a signalling molecule in a wide array of intracellular and extracellular processes, ranging from synaptic activity to intercellular communication and adhesion. Thus, controlled homeostasis of $Ca^{2+}$ is essential for maintaining normal brain physiology and neuronal integrity, ensuring long-term cell survival.

Emerging studies indicate that controlled $Ca^{2+}$ homeostasis is not only critical for cell physiology and overall health but also, when dysregulated, has been associated with several neurodegenerative disorders, including Alzheimer's disease, Parkinson's disease, Huntington's disease, amyotrophic lateral sclerosis, and also Spinocerebellar Ataxia (SCA) (Marambaud *et al*., 2009; Zündorf & Reiser, 2011).

Purkinje neurons, in addition to neurons found in the brainstem and cerebellar nuclei, exhibit high vulnerability to degeneration. Among these, degenerated Purkinje neurons are notably prevalent in cases of SCA. The generation of action potentials in Purkinje neurons relies heavily on the precise and coordinated activity of a diverse array of ion channels to sustain repetitive spiking autonomously. Studies suggest that mutations in genes affecting these ion channel functions can be linked to motor dysfunction in SCA patients (Seidel *et al.,* 2012; Kasumu & Bezprozvanny, 2012).

The *ITPR1* gene, which encodes for the $IP_3$ receptor, is responsible for facilitating the intracellular $Ca^{2+}$ release from the ER stores, has become a significant focus in SCA research. Missense mutations in *ITPR1* are linked to SCA15/16 (Novak *et al.*, 2010) and a recently identified nonprogressive congenital ataxia, SCA29 (Zambonin *et al.*, 2017). Traditionally, mutations in *ITPR1* are linked to the loss of $IP_3$ receptor-channel function. However, it has also been shown that mutations in *ITPR1* can lead to the clinical manifestations of SCA by increasing $Ca^{2+}$ release upon $IP_3$ binding (Hisatsune *et al*., 2018).

In addition, the upstream and downstream molecules involved in ITPR-mediated $Ca^{2+}$ signalling, such as type 1 metabotropic glutamate receptor (mGluR1), transient receptor potential channel C3 (TRPC3), and protein kinase C (PKC), have also been identified as causal genes for SCA 44, 41 and 14, respectively (Huang *et al.*, 2012; Hisatsune *et al*., 2018).

SCA2 is caused by CAG repeats in the *ATXN2* gene, which codes for the ataxin-2 protein. These repeats have been associated with increased sensitivity of ITPR to $IP_3$, causing an enhanced $Ca^{2+}$ release from the ER stores, leading to cell death in cultured Purkinje cells (Hisatsune *et al*., 2018; Kasumu & Bezprozvanny, 2012).

These studies collectively suggest that perturbation in $IP_3R$-mediated $Ca^{2+}$ signalling can be a causal mechanism behind neurodegeneration.

## Hypothesis and Previous Studies

In this project, we aim to study the effects of the two SNPs found in the PITP domain of Nir2 on the protein's function. As a result of the SNPs, glutamine at the 135th position was substituted by proline (Q135P), and the lysine at the 191st position was substituted by glutamic acid (K191E).

Previous studies have used Molecular Dynamics Simulations (MDS) to investigate the effect of non-synonymous SNPs on protein structure and stability in the context of neurodegenerative diseases (Dash et al., 2022). Thus, we decided to perform MDS on a protein-membrane complex (since Nir2 operates at the membrane contact site) to evaluate whether SNPs in the PITP domain of Nir2 have an effect on its overall structure, stability and function.

We hypothesise that these SNPs in the PITP domain of Nir2 could impact the protein's ability to transfer PI from ER to PM, potentially disrupting the PLC-mediated $PIP_2$ signalling. This disruption could lead to a failure in replenishing $PIP_2$ at the PM. Consequently, the reduced concentration of $PIP_2$ and its hydrolysis products, DAG and $IP_3$, may ultimately affect the downstream $Ca^{2+}$ homeostasis of the cells. Perturbed $Ca^{2+}$ homeostasis in the cells could, in turn, contribute to the neurodegenerative phenotypes observed in the patients under our study.

Studies have shown that depletion of Nir2 in cells has a direct correlation with decreased levels of $PIP_2$ and intracellular $Ca^{2+}$ released from the ER stores (***Figure 5***) (Chang *et al*., 2013; Kim *et al.*, 2015)

Based on this knowledge, we decided to use intracellular $Ca^{2+}$ release post PLC stimulation as a readout for Nir2 function and compare this phenotype between HEK cells transfected with Nir2 containing either of the SNPs and wild-type Nir2.

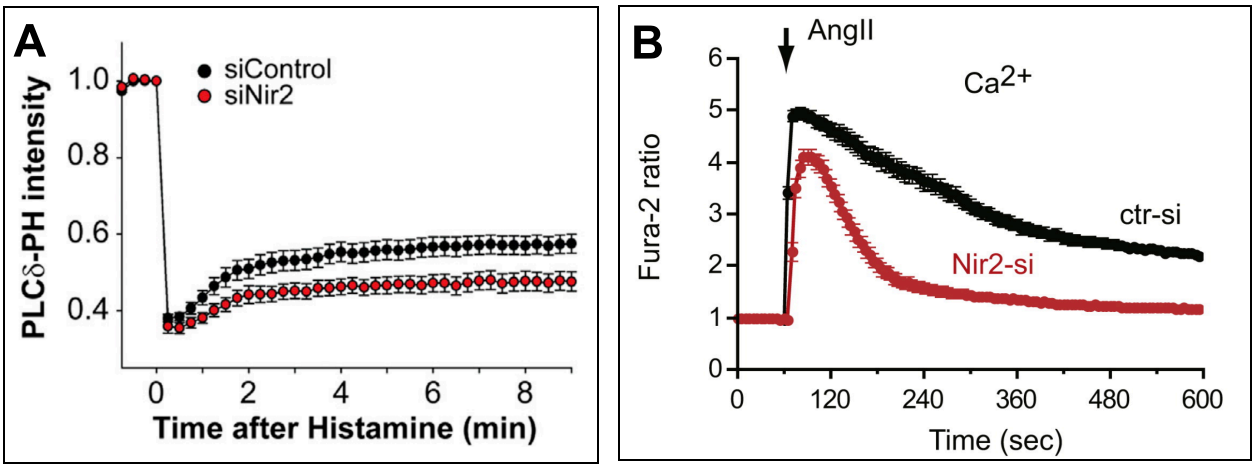


***Figure 5: Effects of Nir2 depletion on $PIP_2$ at PM and intracellular $Ca^{2+}$ (Chang et al., 2013; Kim et al., 2015)***

*(A) Nir2 depletion leads to a decrease in $PIP_2$ levels at the plasma membrane upon agonist (histamine) -mediated PLC stimulation. PLCd-PH intensity is taken as the readout for $PIP_2$. (B) Nir2 depletion leads to a decrease in intracellular $Ca^{2+}$ upon agonist (Angiotensin II) - mediated PLC stimulation.*

# CHAPTER II: AIM AND OBJECTIVES

## Aim

The project aims to evaluate whether SNPs in the PITP domain of Nir2 have a functional effect on the protein. To do this, we divided the project into two components:

First, prior to performing experiments, we assessed the effects of the SNPs on the structure and stability of Nir2 *in silico* by using structure and sequence based prediction methods followed by molecular dynamics simulations to deduce functional changes.

Second, we compared the localisation, expression and function of Nir2 containing patient-specific SNPs with that of wild-type Nir2. We measured intracellular $Ca^{2+}$ release as a functional readout of Nir2.

## Objectives

1. Predict the effects of SNPs on Nir2 structure, stability and function *in silico* by performing molecular dynamics simulations and using prediction tools such as SIFT, Polyphen-2 and FoldX.
2. Clone our gene of interest (mCherry::Nir2) into a mammalian expression vector (pcDNA3.1+).
3. Perform site-directed mutagenesis to generate pcDNA3.1+ clones individually containing patient specific SNPs- mCherry::Nir2-Q135P and mCherry::Nir2 -K191E
4. Overexpress mCherry::Nir2 containing SNPs in HEK-M1 cells and compare changes in expression and localisation with wild-type mCherry::Nir2.
5. Employ PLC-dependent intracellular $Ca^{2+}$ release as a physiological assay to study functional differences between mCherry::Nir2 containing SNPs and wild-type mCherry::Nir2.

# CHAPTER III: MATERIALS AND METHODS

## 1. Sequence Conservation Analysis

### a. UniProt BLAST

The Basic Local Alignment Search Tool of UniProt (The UniProt Consortium *et al.*, 2023) is a comprehensive resource for protein sequence and annotation data. It was used to collect the protein sequences of Nir2 homologs across phyla. The *blastp* program was used, set at default parameters.

### b. Pfam Database

The Pfam Database (Mistry, Jaina *et al.*, 2021) was used to collect the protein sequences of all the PITP domain-containing proteins (~11,000 sequences).

### c. CD-HIT

The CD-HIT algorithm (Fu *et al.*, 2012) was used to cluster protein sequences with a minimum of 90% sequence similarity to reduce redundancy in the sequence data and identify representative sequences (~3,000).

### d. Clustal Omega

Multiple sequence alignment was performed using the Clustal Omega tool (Sievers *et al.*, 2011), set at default parameters.

## 2. *In-Silico* Predictions of the Effects of SNPs

### a. FoldX

FoldX is a computational software tool which can be used for the prediction and analysis of protein stability. The RDGB structure (Krishnan *et al.*, 2023) was used as an input for the FoldX plugin of YASARA (Durme *et al.*, 2011). The *RepairPDB* command was used to perform energy minimisation on the structure. The *BuildModel* command was used to make the amino acid substitutions reported from the patients into protein structure. The *Stability* command was used to calculate the free energy of unfolding ( i.e. $\Delta G$ or the difference in free energy between the unfolded state and the folded state) of the protein. The difference in $\Delta G$ (or $\Delta\Delta G$) between wild-type and variant structures was calculated.

**b. Sorting Intolerant from Tolerant (SIFT)**

SIFT is a bioinformatics tool used to predict the impact of amino acid substitutions on a protein's function based on evolutionary conservation.The protein sequence of wild-type Nir2 and the amino acid substitutions (caused by the SNPs in patients) were used as an input for SIFT (Ng & Henikoff, 2003). The median conservation of sequences was set to 3, and the sequence identity threshold was set to 90%. A SIFT score was generated for each of the amino acid substitutions based on sequence homology. If the score is <= 0.05, then the substitution is predicted to be damaging, else it is predicted to be tolerated by the protein.

**c. Polyphen-2**

Polyphen-2 is a bioinformatics tool used to predict the effect of amino acid substitutions on the protein's structure and function based on evolutionary conservation, physicochemical properties, and structural information. The protein sequence of wild-type Nir2 and the amino acid substitutions were used as an input for PolyPhen-2 (Adzhubei *et al.*, 2013). The *HumDiv* classifier model was used to produce predictions as a score which could fall between 0 and 1, categorising the substitutions into three categories: benign, possibly damaging, and probably damaging. The substitution is predicted to be benign if the score is closer to 0 and damaging if the score is closer to 1.

## 3. Molecular Dynamics Simulations

**a. CHARMM-GUI**

The *Membrane Builder* module of CHARMM-GUI was used to generate input structures for the molecular dynamics simulations. The RDGB structure was placed 10 nm away from a dipalmitoylphosphatidylcholine (DPPC) membrane containing 250 lipid molecules, each in the upper and lower leaflets. The entire protein-membrane complex was then solvated with water molecules and neutralised with $K^+$ and $Na^+$ ions to obtain a net zero charge.

**b. GROMACS**

The protein-membrane complex was used as an input for GROMACS (Berendsen *et al*., 1995). The simulations were conducted employing a step size of 2 fs, and the nearest neighbour list was logged every 20 ps. Temperature and pressure were controlled at 300K and 1 $bar^{-1}$, respectively. The complex was energy minimised until convergence over a period of 50 ns, followed by six equilibration steps, each lasting 50 ns. Subsequently, the final molecular dynamics (MD) run, utilising the charmm36m force field, was performed for 100 ns (in replicates). The RMSD and RMSF were computed using the *gmx rms* and *gmx rmsf* commands, respectively, while the minimum distance between the protein and membrane was determined using the *gmx mindist* command.

**c. PyMOL**

PyMOL (The PyMOL Molecular Graphics System, Version 2.0 Schrödinger, LLC) was used to visualise protein structures and protein-membrane complexes pre and post-simulation.

**d. QtGrace**

QtGrace (v0.2.7) was used to generate RMSD, RMSF and minimum-distance plots.

**4. <u>Gene Cloning</u>**

Gibson Cloning was attempted to clone our gene of interest (mCherry::Nir2) in our desired mammalian expression vector (pcDNA3.1+). The gene mCherry::Nir2 was cloned from an existing plasmid in the lab- pUAST-attB-mCherry::Nir2 using the following Gibson primers (designed using NEB Interactive Tools):

Forward 5’ - TAAGCTTGGTACCGAGCTCGGATCCATGGTGTCCAATTTCGAAGAG - 3’

Reverse 5’ - GACCTGTCGCTCCTCCCTATTGAGCTCAGATCTCCCGGGCAAATTT - 3’

Amplified mCherry::Nir2 insert and a linearised pcDNA3.1+ vector were separately run on a 1.5% agarose gel to confirm that they were intact prior to cloning by Gibson

Assembly. The Gibson Assembly products were transformed into competent *E. coli* DH5α cells. Multiple colonies (~17 colonies) were randomly selected and screened for the presence of the desired mCherry::Nir2 construct by colony PCR using the following primers:

Forward 5’ - GGCCCGCCTGGCATTATGCC - 3’

Reverse 5’ - GGCCCGCCTGGCATTATGCC - 3’

Double digestion (using BamHI and XhoI) was performed to verify the release of the desired gene from the newly cloned vector. The gene sequence was verified using Sanger Sequencing.

**5. <u>Site-Directed Mutagenesis (SDM)</u>**

We employed site-directed mutagenesis (SDM) to generate pcDNA3.1+ clones individually, having mCherry::Nir2 with SNP Q135P and mCherry::Nir2 with SNP K191E. These SNPs corresponded to the patient-specific mutations in Nir2. SDM was carried out using commercially synthesised mCherry::Nir2-pcDNA3.1+ clone as a template and using primers:

Q135P Forward 5’ - GGGCCGAGAGGAGACCGCGCATCCTGGACAC - 3’

Q135P Reverse 5’ - GTGTCCAGGATGCGCGGTCTCCTCTCGGCCC - 3’

K191E Forward 5’ - CTTATGTGTGCCTATGAGCTGTGCAAGGTTG - 3’

K191E Reverse 5’ - CAACCTTGCACAGCTCATAGGCACACATAAG - 3’

The gradient PCR was set up with three different annealing temperatures according to the respective primer melting temperatures (Tm). After that, the template DNA was subjected to DpnI digestion, post which the PCR product was transformed into competent DH5α cells. Multiple colonies (~10 colonies) were screened, and the plasmids isolated from these colonies were submitted for Sanger sequencing to verify the sequence and confirm the presence of the desired point mutation.

## 6. Mammalian Cell Culture and Transfection

### a. DNA Constructs

We had an existing recombinant HEK293T cell line (HEK-M1 cells) in the lab that constitutively expressed the muscarinic acetylcholine receptor M1 (m1AchR). This system allowed a controlled stimulation of the PLC by the addition of the agonist Carbamoylcholine chloride (or Carbachol; Cch). In the background of these HEK-M1 cells, Nir2 shRNA and Nir2 scrambled shRNA were transduced to generate HEK-M1-Nir2 shRNA (Nir2 depleted cells) and HEK-M1-Scrambled shRNA line (Control cells), respectively. Both constructs were previously generated in the lab (Saha *et al.*, 2023) and had been packaged in second-generation lentiviral capsids for transduction. Both the cell-lines- HEK-M1-Nir2 shRNA cells and the HEK-M1-scrambled shRNA cells were selected via Puromycin selection (1.2 µg/ml) since the constructs were cloned in pGIPZ vectors having Puromycin resistance cassettes (GE Dharmacon).

### b. Cell Maintenance

Cells were maintained under standard conditions at 37°C, with 5% $CO_2$ in Dulbecco's Modified Eagle Medium (DMEM), high Glucose media (HiMedia), supplemented with sodium bicarbonate and 10% Foetal bovine serum (FBS) along with Streptomycin and Penicillin antibiotics (SIGMA; G1146).

### c. Transfection

Transfection with WT mCherry::Nir2 or mCherry::Nir2 constructs with either of the mutations (K191E or Q135P) was done using Lipofectamine™ 3000 Transfection Reagent (ThermoFisher Scientific) when the cells were 60-70% confluent as per manufacturer's protocol.

## 7. Western Blotting

Post-transfection, the cells were harvested after 36-48 h and lysed in an appropriate volume of protein lysis buffer supplemented with 1X protease inhibitor cocktail (PIC). Total protein content in lysates was estimated using Bradford assay (BioRad), and the corresponding volumes for 20 µg of total protein was calculated. The protein samples were mixed with 2X Laemmli's buffer, heated at 95$^{o}$ C for 5 min and then loaded and

separated on 10% SDS-PAGE gel. The proteins were then transferred onto a nitrocellulose membrane (Amersham) (via wet transfer system; BioRad) and then blocked with 10% Blotto (Santa Cruz Biotechnology) diluted in Tris Buffer Saline containing 0.1% Tween-20 (0.1% TBST) for 30 min. Subsequently, the membrane was incubated with rabbit anti-mCherry antibody (1:1,000 diluted in 5% BSA in 0.1%TBST) (PA5-34974; Thermo Fisher Scientific) overnight at 4°C. For loading control, the blot was incubated with mouse anti-β-tubulin antibody (1:4,000 diluted in 5% BSA in 0.1% TBST) (DSHB Hybridoma Product E7). The blots were then washed thrice with 0.1% TBST and incubated with the appropriate HRP-conjugated secondary antibodies (1:10,000 dilutions; Jackson Laboratories, Inc.) for 2 h. Post incubation with the secondary antibodies, the blot was washed thrice with 0.1% TBST and developed using Clarity Western ECL substrate (Bio-Rad) on a GEImageQuant LAS 4000 system. Images were analysed using ImageJ (open source).

**8. <u>Calcium Imaging</u>**

**a. Fluorescence Imaging**

Cells were seeded in Matrigel, Growth Factor Reduced (Corning, C354277) coated cover-slip dishes. 24 h post transfection, cells were washed twice with HBSS buffer (10 mM HEPES, 118 mM NaCl, 1.18 mM $MgSO_4$, 4.96 mM KCl, 1.18 mM $KH_2PO_4$, 2 mM $CaCl_2$, 10 mM Glucose; pH-7.4) and then loaded with the ratiometric $Ca^{2+}$ indicator Fura-2 AM (4 μM) (excitation 340/380 nm, emission 510 nm) (Acetoxymethyl Ester; Invitrogen) along with 0.002% Pluronic F-127 for 30 min at 25°C. Cells were then washed twice with HBSS to remove the excess dye. Cells were then incubated in HBSS at room temperature for 20 min to allow de-esterification of intracellular dye. Imaging was performed using a 20X objective of Olympus IX-83 wide-field fluorescence microscope for the duration of 10 min. Fluorescence intensities of both free and $Ca^{2+}$ bound Fura-2 fluorescence intensities were recorded at every 5 s interval using an EM-CCD camera (Evolve 512 Delta; Photometrics). The initial 18 frames were recorded to determine the basal cytosolic $Ca^{2+}$ of the cells. The next 42 frames were recorded after adding Carbamoylcholine chloride (20 μM) (C4382;

Sigma-Aldrich), used to activate PLC, thereby inducing $Ca^{2+}$ release from the ER stores. The next 24 frames were recorded after adding Ionomycin (20 µM) (Calbiochem), used to induce $Ca^{2+}$ entry across the plasma membrane and determine the $R_{max}$. Lastly, 24 frames were recorded after adding EGTA (4 mM), used to chelate $Ca^{2+}$ ions and determine the $R_{min}$ (***Figure 6***).

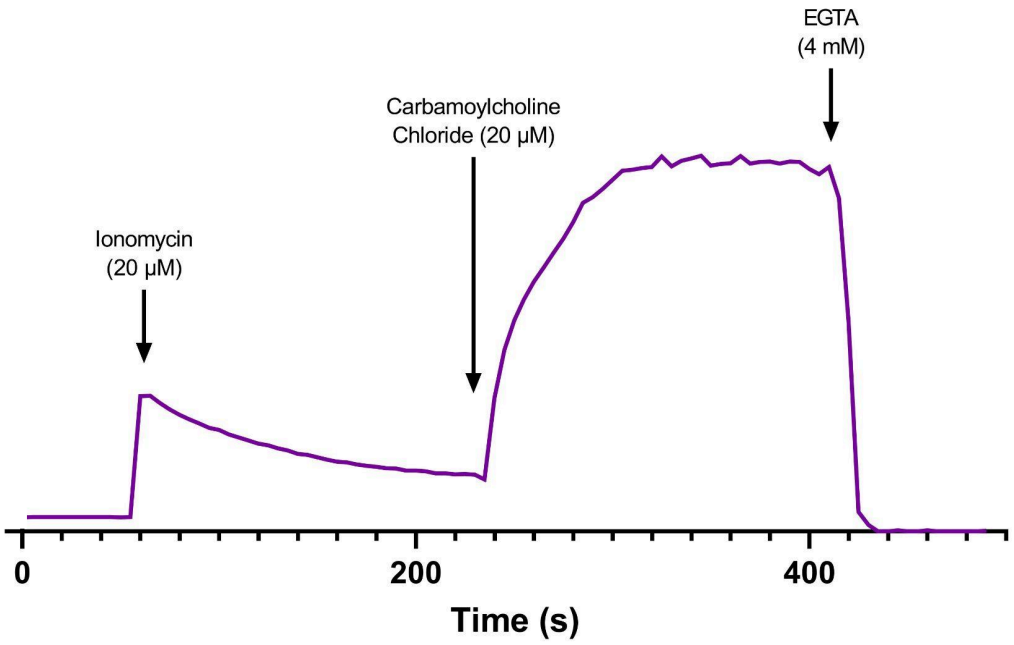


***Figure 6: $Ca^{2+}$ Imaging experiment protocol***
*Carbamoylcholine chloride (20 µM) is used to activate PLC signalling, Ionomycin (20 µM) is used to determine the $R_{max}$, EGTA (4 mM) is used to determine $R_{min}$.*

**b. Analysis**

For each cell, a dynamic region of interest (ROI) was drawn using the CellSens Olympus software. Fluorescence intensities measured from these ROIs reflected the temporal variations in the intracellular $Ca^{2+}$ ($[Ca^{2+}]_i$). By analysing the emission intensities corresponding to 340 nm and 380 nm excitations, the 340/380 ratio was calculated for each cell at every time point. The Grynkiewicz equation (Grynkiewicz *et al*., 1985) was then applied to estimate the $[Ca^{2+}]_i$:

$$[Ca^{2+}]_i\,(nM) = K_d \times SF \times [(R - R_{min})/(R_{max} - R)]$$

where $R_{max}$ and $R_{min}$ refer to the maximum and minimum 340/380 ratio, respectively. 224 nM was taken as $K_d$ for Fura-2 AM in human cells, and SF (scaling factor) was calculated for each cell by dividing the fluorescence emission intensity of the dye at $Ca^{2+}$ free form with the fluorescence emission intensity at $Ca^{2+}$ bound form after excitation at 380 nm. The final traces of $Ca^{2+}$ mobilisation were plotted using GraphPad Prism 9.0. Normal distribution was checked for the data points and then Student's t-test and one-way ANOVA were used to compare the means between the samples of different genotypes.

**9. <u>Localisation Studies</u>**

Cells were seeded in Matrigel, Growth Factor Reduced (Corning, C354277) coated cover-slip dishes.

**a. Nir2 at Basal State**

24 h post transfection, cells were fixed with 4% PFA (dissolved in HBSS) on ice for 20 mins. Upon fixation, cells were washed thrice with HBSS and permeabilised with 0.5% Triton-X (dissolved in HBSS). Following this, in order to stain the nucleus, cells were incubated with DAPI (1:3,000 dilution; dissolved in HBSS) for 10 minutes at RT. The excess stain was removed by washing the cells twice with HBSS. Imaging was performed using a 60X oil immersion objective of Olympus FV 3000 confocal microscope. Images were analysed using ImageJ (open source).

**b. Immunocytochemistry Post PLC Activation**

24 h post transfection, the GPCR-mediated PLC signalling pathway was activated by carbamoylcholine chloride (120 µM) addition. 3 minutes post addition, cells were fixed with 4% PFA (dissolved in HBSS) on ice for 20 mins. Cells were then washed twice with HBSS and permeabilised with 0.5% Triton-X (dissolved in HBSS). Following this, cells were incubated with blocking solution (5% Bovine Serum Albumin (BSA) diluted in TBS) for 1 h at RT. Cells were incubated overnight at 4°C with mouse anti-mCherry antibody (Thermo Fisher Scientific; MA5-47384) at a 1:500 dilution in 5% BSA in 0.1% TBST and rabbit

anti-STIM1 antibody (Cell Signalling Technology; 5668) at a 1:500 dilution in 5% BSA in 0.1% TBST. After washing thrice with 0.1% TBST, cells were incubated with secondary antibodies anti-mouse Alexa Fluor 568 (Thermo Fisher Scientific; A11004) at a 1:300 dilution in 5% BSA in 0.1% TBST and anti-rabbit Alexa Fluor 488 (Thermo Fisher Scientific; A11034) at a 1:300 dilution in 5% BSA in 0.1% TBST at RT for 2 hours. Cells were finally washed three times with TBS. Imaging was performed using a 60X oil immersion objective of Olympus FV 3000 confocal microscope. Images were analysed using ImageJ (open source).

## CHAPTER IV: RESULTS

### 1. *In Silico* Predictions Reveal both the SNPs in the PITP Domain are Deleterious to Nir2 Function

Single nucleotide polymorphisms (SNPs) were reported in the Nir2 encoding *PITPNM1* gene in patients displaying symptoms indicative of cerebellar dysfunction. We received the data regarding the amino acid substitutions present in the Nir2 protein as a result of these SNPs from seven different patients (***Figure 7***). Of these seven patients, two had SNPs in the PITP domain, which were picked for further studies.

The PITP domain facilitates the binding and transfer of phosphatidylinositol (PI) and phosphatidic acid (PA) across the subcellular membranes, thereby playing a crucial role in maintaining the PI signalling of the cell (Kim *et al.*, 2015). Thus, SNPs in this domain could affect Nir2 function upon activation of PLC.


***Figure 7: Domain architecture of the human PITPNM1 gene annotated with the SNPs reported in patients of spinocerebellar ataxia.***

The glutamine at the 135th position (Q135) was substituted by proline, and the lysine at the 191st position (K191) was substituted by glutamic acid. Studies suggest that SNPs leading to amino acid substitutions in evolutionarily conserved positions are likely to affect protein function (Miller and Kumar, 2001). We performed a protein BLAST on the UniProt database to collect a total of 102 protein sequences of Nir2 homologues across phyla. Multiple sequence alignment results revealed that both the residues under analysis in this study were largely conserved (***Figure 8***).


***Figure 8: Representative multiple sequence alignment of Nir2 homologues across phyla (28/102)*** *Both Q135 and K191 are highly conserved residues across phyla.*

Similarly, we collected ~11,000 protein sequences of all the PITP domain containing proteins from the Pfam database to perform a more elaborate analysis of the phylogenetic conservation of our residues of interest. We used the CD-HIT algorithm to cluster protein sequences with a minimum of 90% similarity to reduce redundancy in the sequence data and identify ~3,000 representative sequences. Multiple sequence alignment results revealed that Q135 was conserved in 20.6% of sequences, while K191 was conserved in 86.2% (***Figure 9***).


***Figure 9: Representative multiple sequence alignment of PITP domain-containing proteins (30/3000)***

*Both Q135 and K191 are conserved residues, with K191 showing higher (86.2%) conservation than Q135 (20.6%).*

The above alignment results provide collective evidence supporting the rarity of the patient SNPs, with both residues displaying conservation. Notably, K191 exhibits a higher degree of conservation across PITP domain-containing proteins compared to Q135.

For further validation, we used an online prediction tool called SIFT to predict the effect of the patient-specific SNPs on protein function. Using the principle of sequence conservation, SIFT calculates a score for each mutation, ranging from 0 to 1. A score <= 0.05 indicates that the substitution is prone to intolerance by the protein, meaning it may affect the protein's function. Conversely, a score > 0.05 suggests that the substitution is likely to be tolerated, implying that it might not affect the protein's function. In our analysis, SIFT predicted that the Q135P substitution would be tolerated by the protein. On the other hand, it predicted that the K191E substitution would not be tolerated by the protein and would likely affect the protein function (***Table 1***).

The position of the substituted amino acid within the structure of the protein can also give us information on whether or not it is crucial for the protein's function. For example, if the residue is located in a region that is more prone to mutations, it might not be vital for the protein's function. Based on this hypothesis, we used another prediction tool called Polyphen-2 to predict the effects of the SNPs based on information about structure and sequence conservation. Polyphen-2 makes predictions as a score that falls between 0 and 1. It also reports an associated false positive rate that is used to qualitatively evaluate the SNPs as benign, possibly damaging or probably damaging. In our analysis, Polyphen-2 predicted both Q135P and K191E substitutions to be "Probably Damaging" to the protein's stability and function (***Table 1***).

| | **Q135P** | **K191E** |
|---|---|---|
| **SIFT** | 0.07 | 0.00 |
| | Tolerated | Affect Protein Function |
| **PolyPhen-2** | 0.997 | 0.996 |
| | Probably Damaging | Probably Damaging |

***Table 1: SIFT and Polyphen-2 predictions***
*SIFT predicted K191E substitution to be deleterious to the protein function. Polyphen-2 predicted both Q135P and K191E substitutions to be deleterious to the protein function.*

Nir2 protein sequence was used to predict all the above results. In order to make more accurate and advanced predictions, we needed to use the Nir2 structure as an input for subsequent prediction tools. However, a 3-D structure of the Nir2 protein was not available. Due to 67.5% similarity in the PITP domain of Nir2 and RDGB protein (***Table 2***), we used the full-length model of the RDGB, previously generated in the lab (Krishnan *et al.*, 2023), for the rest of our studies.

| Full-Length | PITP | LNS2 | DDHD |
|---|---|---|---|
| 46.88% | 67.47% | 63.36% | 50.82% |

***Table 2: Sequence alignment results of Nir2 and RDGB.***
*The PITP domain of Nir2 and RDGB share 67.47% similarity.*

Nir2 and RDGB protein sequences were aligned, and the corresponding amino acid substitutions caused by the patient-specific SNPs were annotated in RDGB (***Table 3***). These were used as inputs for all the downstream analyses.

| S. No. | Gene | Protein (Nir2) | Protein (RDGB) |
|---|---|---|---|
| 1 | 404A>C | Gln135Pro (Q135P) | Asn135Pro (N135P) |
| 2 | 571A>G | Lys191Glu (K191E) | Lys202Glu (K202E) |

***Table 3: Patient SNPs and their corresponding amino acid substitutions for Nir2 and RDGB.***

Using the FoldX plugin of YASARA, we incorporated patient-specific SNPs into the RDGB structure and calculated the free energy of unfolding ($\Delta G$) of the wild-type and variant proteins (***Table 4***). We observed a positive difference in $\Delta G$ between the variant and wild-type structures, indicating that the substitutions might have a destabilising effect on the protein. Interestingly, K191E showed a higher difference, indicating a higher degree of destabilisation.

| | Free Energy of Unfolding ($\Delta G$) | Difference ($\Delta\Delta G = \Delta G_{Variant} - \Delta G_{WT}$) | Result |
|---|---|---|---|
| **WT RDGB** | 3168.81 kcal/mol | - | |
| **WT RDGB (Repaired)** | 1882.81 kcal/mol | - | |
| **Q135P** | 1883.1 kcal/mol | 0.29 kcal/mol | Mutation is Destabilising |
| **K202E** | 1883.66 kcal/mol | 0.85 kcal/mol | Mutation is Destabilising |

***Table 4: FoldX Predictions***
*Positive difference in ΔG between variants (both Q135P and K191E) and WT RDGB structures, predicting the substitutions to have a destabilising effect on protein structure.*

**2. <u>Molecular Dynamics Simulation Results Predict K191E SNP Affects Structural Stability and Function of Nir2</u>**

We investigated the membrane interaction and binding properties of the RDGB protein using molecular dynamics (MD) simulations. We incorporated patient-specific amino acid substitutions into the full-length RDGB model. We then placed the protein model 10 nm above a dipalmitoylphosphatidylcholine (DPPC) membrane. The system (protein-membrane complex) was subjected to energy minimisation, six steps of equilibration, followed by the MD run for 100 ns.

Following the simulation, we performed structural alignment of the protein (WT and variants) at 0, 50 and 100 ns of the trajectory to identify any changes in the structure and overall stability of the complex. We observed minimal alterations in the protein-membrane interaction for the N135P substitution, closely resembling the WT. Conversely, the K202E substitution induced large movements between the protein and the membrane, leading to large structural changes in the protein (***Figure 10***).

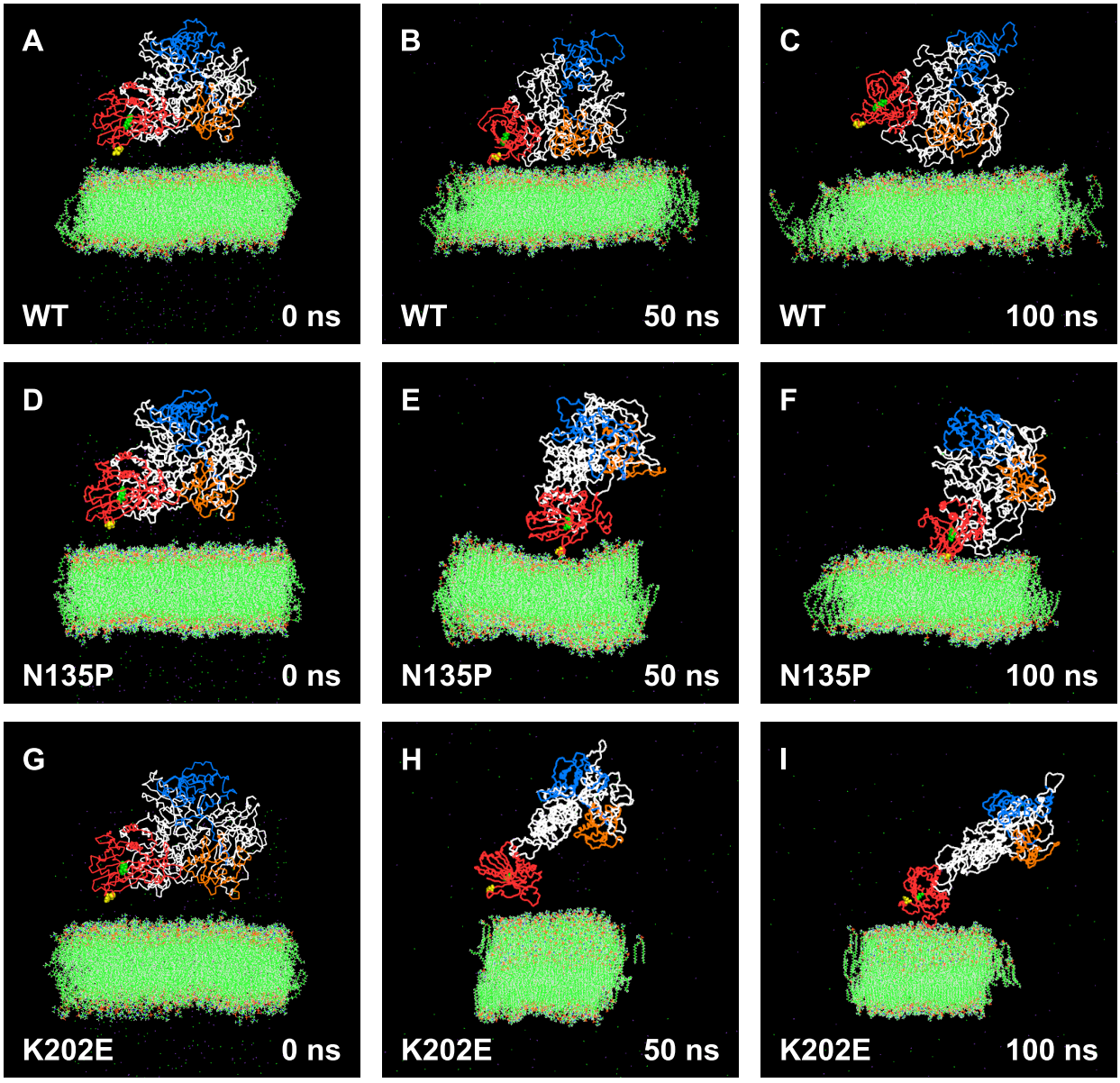


***Figure 10 : Structural alignment of the protein-membrane complex***

*No significant difference in the structure of the WT protein-membrane complex over the course of simulation at 0 ns (A), 50 ns (B) and 100 ns (C). Minimal difference in structure of Q135P variant over the course of simulation at 0 ns (D), 50 ns (E) and 100 ns (F). A significant difference in the structure of the K202E variant over the course of the simulation at 0 ns (G), 50 ns (H) and 100 ns (I). The PITP domain, LNS2 domain and DDHD domain are annotated with red, orange and blue colours, respectively.*

We generated Root Mean Square Deviation (RMSD) plots to measure the difference between the backbone of the protein from its initial structural conformation over the course of the trajectory. The protein's stability can be evaluated based on the deviations observed during the simulation. We observed that the N135P substitution exhibited minimal deviation and stabilised at the level of ~1.4 Å after 20 ns. In contrast, the K202E substitution led to a higher and sustained deviation at an average level of ~2.8 Å. The RMSD plot showed that the N135P variant maintained overall stability throughout 100 ns of simulation, while the K202E variant displayed more fluctuations, signifying a greater impact on the protein stability (***Figure 11A***).

We also generated Root-Mean-Square-Fluctuation (RMSF) plots to calculate how much an individual residue fluctuates during a simulation. In general, regions with higher RMSF values indicate lower stability, as they experience less movement or deviation from their average position during the simulation, and vice versa. We observed that the 135th residue of the N135P variant does not fluctuate significantly, showing modest differences in movement (~2.6 Å ) as compared to the WT. On the other hand, the 202nd residue of the K202E variant shows high fluctuation, with a much higher difference in movement (~8.6 Å), as compared to the WT (***Figure 11B***).

Finally, we plotted the minimum distance between the RDGB protein and the membrane, measured over the course of the 100 ns run. This was done to understand the membrane binding and interaction properties of the variants compared to the WT. We hypothesised that a greater distance between the protein and membrane would suggest improper localisation of the protein and, thereby, a reduced interaction. This, in turn, could affect the protein function. We observed that the N135P variant stabilises after 30 ns, and shows only minimal changes in the membrane-protein distance compared to the WT. On the other hand, a significant increase in this distance is observed with the K202E substitution, indicating its potential impact on the function (***Figure 11C***).

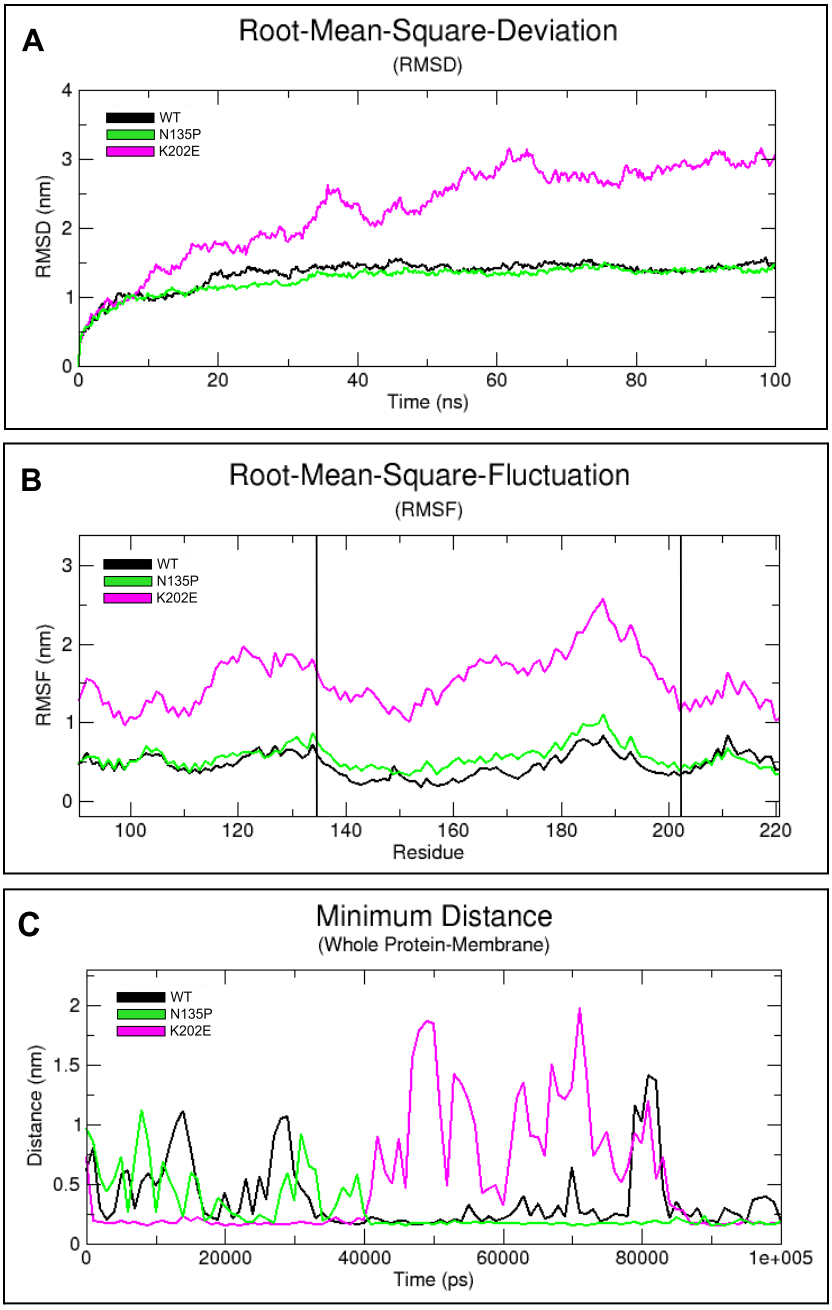


***Figure 11: RMSD, RMSF and Minimum-Distance plots***

*(A) RMSD values of WT and N135P variant stabilise after 20 ns, whereas K202E variant displays a sustained increase in deviation. (B) RMSF value of the 135th residue of N135P variant shows minimal difference in fluctuation (~2.6 Å) compared to WT. The 202nd residue of the K202E variant shows a significant difference in fluctuation (~8.6 Å). (C) Minimum distance (protein-membrane) plots of WT and N135P variant stabilise after 30 and 40 ns. The K191E variant induces large movements between the protein and membrane and does not stabilise over time.*

## 3. Gene Cloning and Incorporation of Patient-Specific SNPs in HEK-M1 Cells

*In silico* results predicted that both the SNPs (K191E more than N135P) in the PITP domain of Nir2 might have a deleterious effect on the protein's function. Previous studies have suggested that non-synonymous SNPs in genes can affect the expression or localisation of the translated protein in cells (Yates & Sternberg, 2013). This, in turn, could have pathological effects. To test this, we decided to compare the localisation and expression levels of the Nir2 having SNPs with the WT Nir2. We decided to use HEK-M1 cells as our model system and transfected them individually with pcDNA3.1 constructs either having WT mCherry::Nir2 or mCherry::Nir2 having the SNPs to check for localisation and expression levels of the proteins.

We attempted to clone mCherry-tagged Nir2 (mCherry::Nir2) into a pcDNA3.1+ mammalian expression vector via Gibson Assembly. Amplified mCherry::Nir2 (from pUAST-attb-Nir2-mCherry) and the linearised pcDNA3.1+ vector were separately run on an agarose gel, and bands of expected size were observed, confirming that both the insert and vector were intact (***Figure 12***).

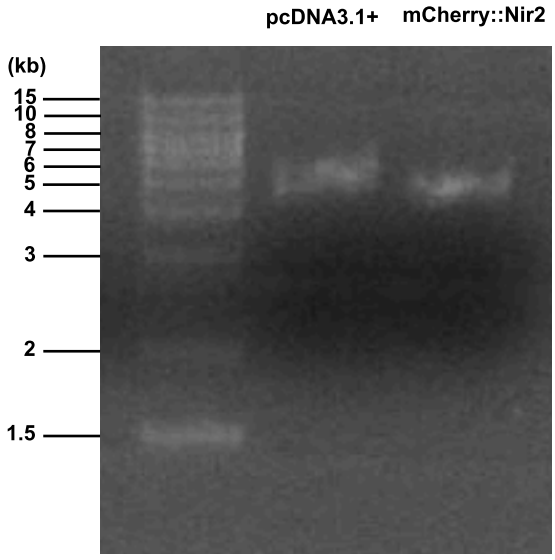


***Figure 12: Verification of fragments for Gibson assembly***
*Linearised and double digested vector (pcDNA3.1+) band at an expected size of 5.5 kb. Amplified, gel-purified and double digested insert (mCherry::Nir2) band at an expected size of 4.5 kb.*

We transformed competent *E. coli* DH5α cells with the Gibson Assembly product and screened 17 individual colonies for the presence of the desired mCherry::Nir2-pcDNA3.1+ construct by performing colony PCR. We observed that colony 13 was positive for the screen (***Figure 13***).

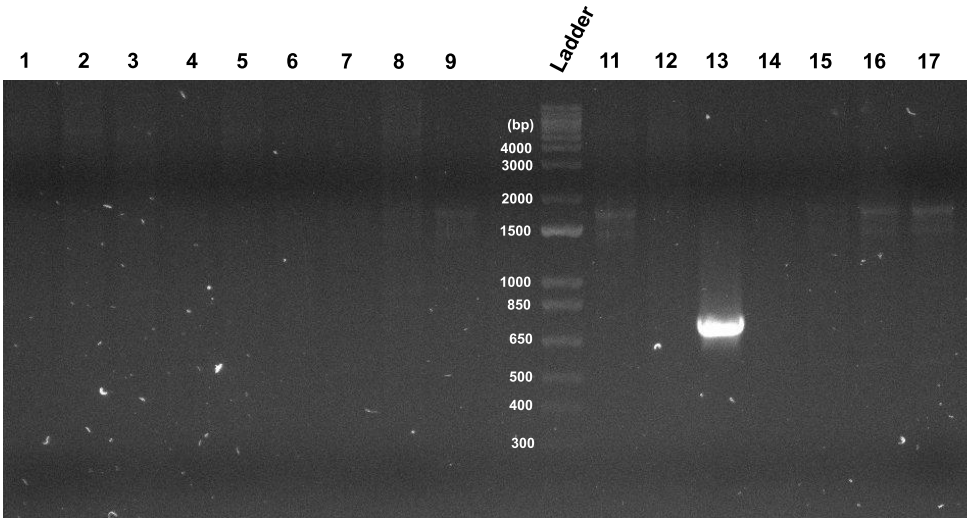


***Figure 13: Colony PCR***
*Out of the 17 colonies screened, only colony 13 yielded the colony PCR amplicon at the expected size of 700 bp.*

However, upon verifying the sequence of the plasmid isolated from colony 13 by Sanger Sequencing, we observed that some parts of the insert had not been integrated into the vector, possibly due to random recombination events. After several troubleshooting experiments, we decided to get our construct (mCherry::Nir2-pcDNA3.1+) commercially synthesised.

We transfected HEK-M1 cells with our newly synthesised mCherry::Nir2-pcDNA3.1+ construct(mCherry::Nir2 from hereon). 24 hours post-transfection, mCherry fluorescence confirmed Nir2 expression (***Figure 14***). Untransfected HEK cells, used as a negative control, showed minimal fluorescence.

We then performed site-directed mutagenesis to construct the two patient-specific SNPs- Q135P and K191E- individually into the mCherry::Nir2 construct. We verified the successful incorporation of the SNPs by Sanger Sequencing (***Figure 15***).

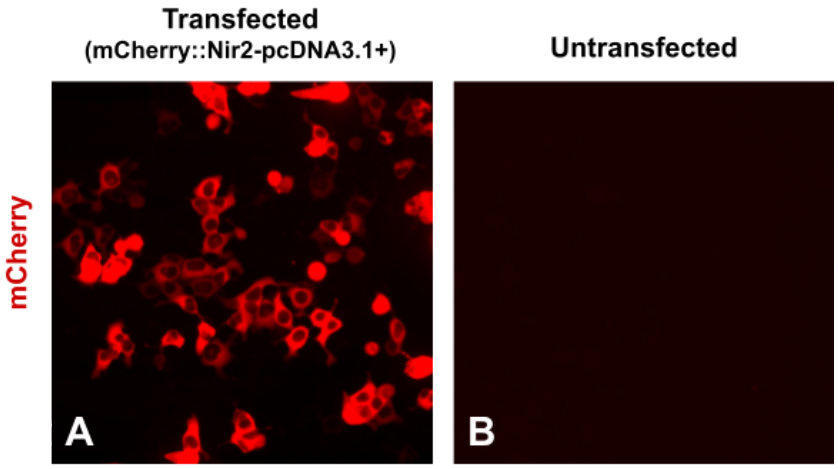


***Figure 14: Construct verification by transfection***

*(A) Fluorescence in the mCherry channel for HEK 239T cells transfected with mCherry::Nir2-pcDNA3.1+ construct. (B) No fluorescence signal in the untransfected HEK-M1 cells (negative control).*

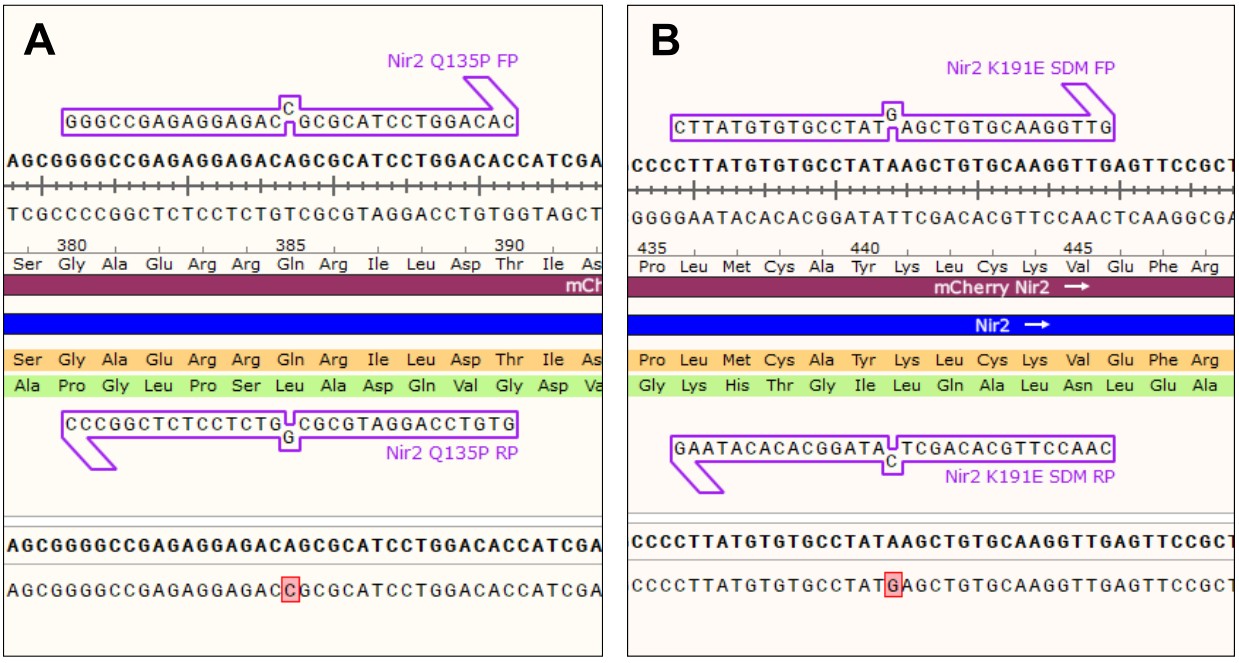


***Figure 15: Verification of successful incorporation of SNPs***

*Sequence of mCherry::Nir2 having the SNP (A) Q135P, which led to the replacement of Glutamine by Proline at the 135th position and (B) K191E, which led to the replacement of Lysine by Glutamic Acid at the 191st position.*

## 4. Protein Localisation of both the Variants is Similar to WT Nir2

To validate the effect of variants (K191E and Q135P) on Nir2 localisation, we independently overexpressed Nir2::mCherry containing patient-specific SNPs by transient transfection. The recombinant HEK 293T cell line, generated previously in the lab, expressing the muscarinic acetylcholine receptor M1 (m1AchR) (Saha *et al.*, 2023) was used for the same and will be referred to as the HEK-M1 cells. Confocal microscopy experiments revealed that at the basal state (when m1AchR is inactive), WT Nir2 exhibited diffused cytoplasmic localisation patterns (potentially ER and Golgi (Kim *et al.*, 2015; Litvak *et al.*, 2002)). Interestingly, both variants of Nir2 also exhibited a similar localisation pattern (***Figure 16***). The mCherry fluorescence was taken as a readout for Nir2 expression.

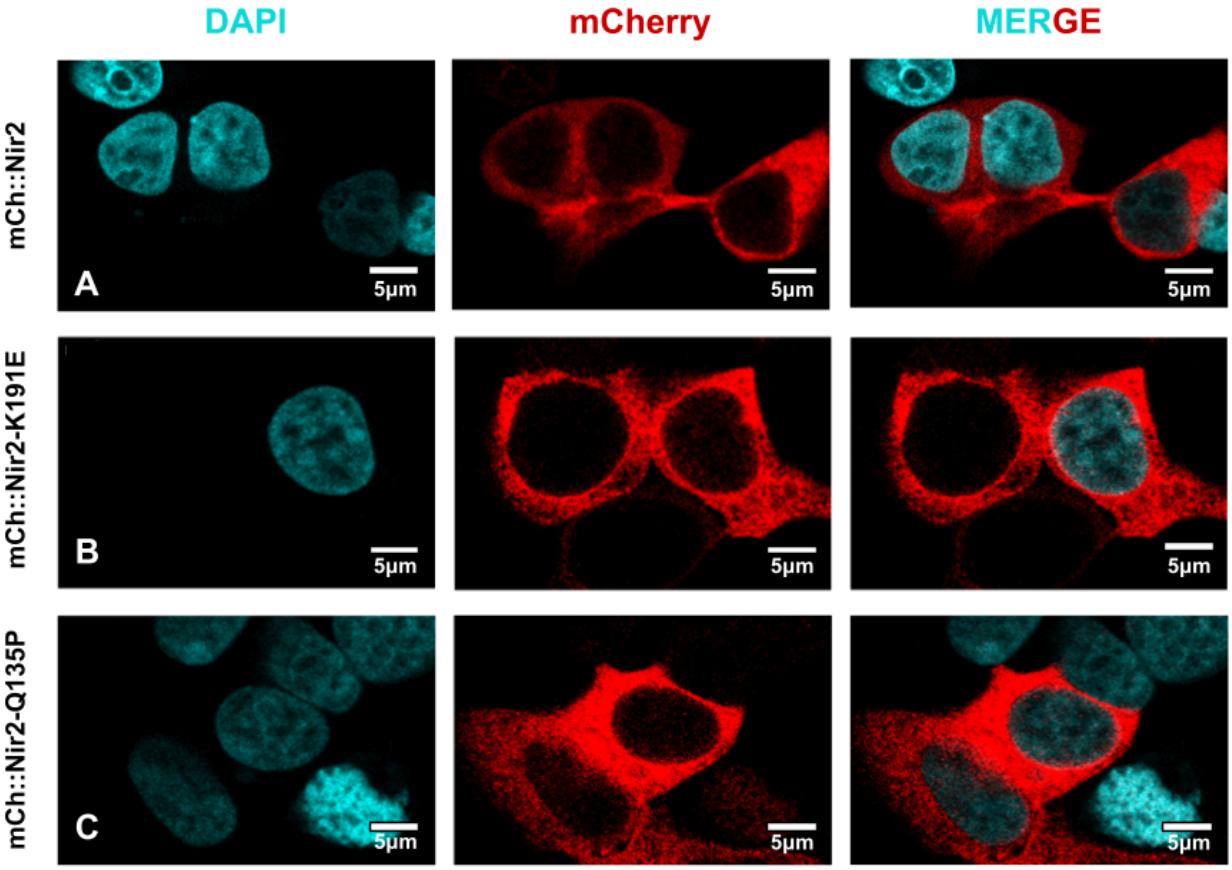


***Figure 16: Comparison of protein localisation at basal state***
*Nir2 Localisation pattern in HEK-M1 cells for the variants (B) K191E and (C) Q135P was similar to (A) WT. The nucleus was stained with DAPI (blue).*

After observing no alterations in the localisation of the variant Nir2 proteins at the basal state, we decided to study Nir2 localisation in PLC-activated cells. Upon treatment of cells with Carbamoylcholine chloride (Cch) for 3 mins (to activate PLC signalling via m1AchR), we observed that Nir2 translocates to ER-PM contact sites and co-localises with Stim1, a known ER-PM junction protein. Consistent with our previous findings, both Nir2 variants exhibited similar localisation patterns as compared to WT Nir2 (***Figure 17***).

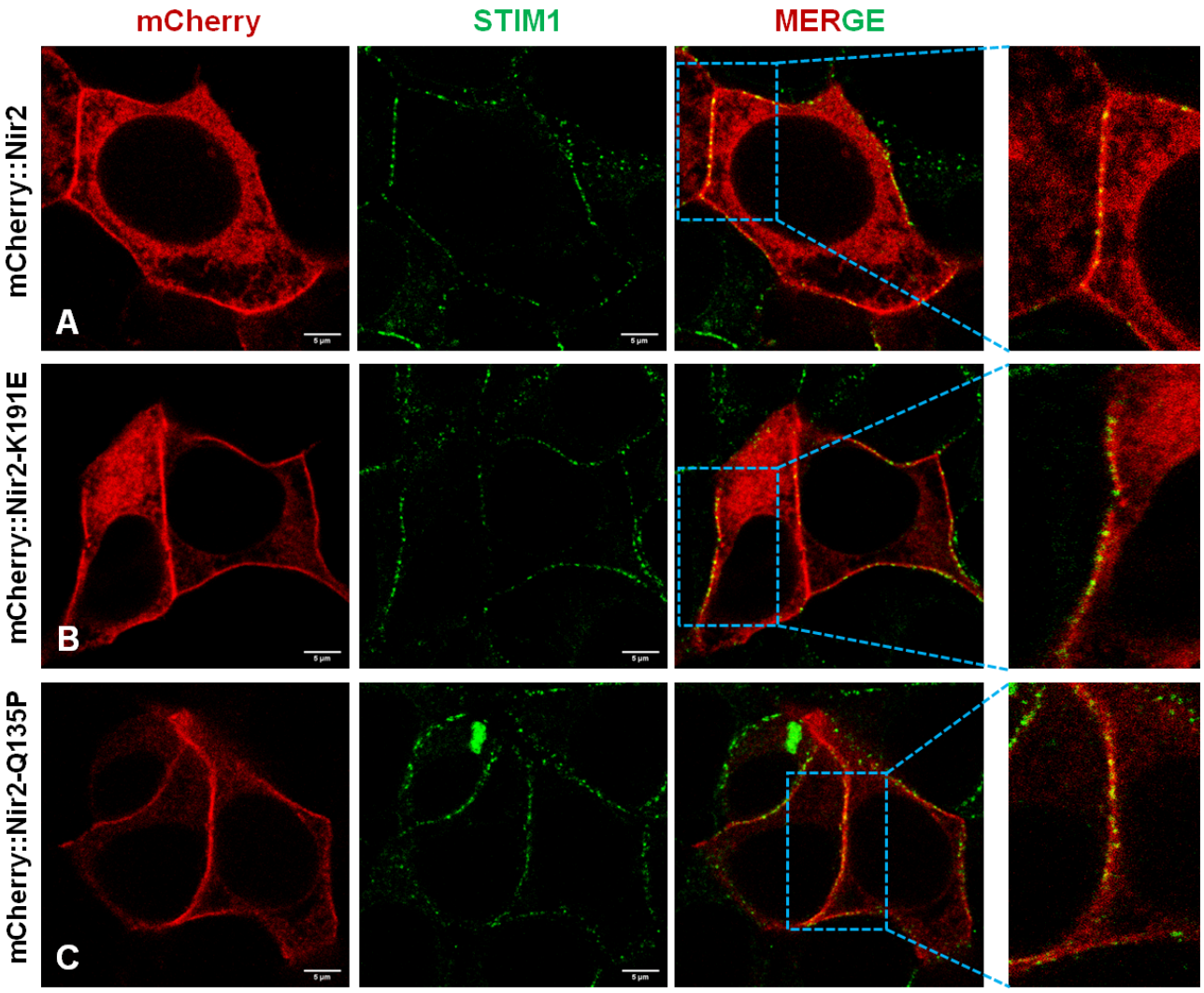


***Figure 17: Comparison of protein localisation following PLC activation***
*Following PLC stimulation, Nir2 co-localises with ER-PM contact sites as marked by Stim1 proteins. The co-localisation pattern of Nir2 in HEK-M1 cells for the variants (B) K191E and (C) Q135P was similar to (A) WT. Enlarged overlay of the ER-PM contact sites is indicated by the blue box.*

## 5. Protein Expression of both the Variants is Similar to WT Nir2

Protein level estimation via Western blotting revealed that both the Nir2 variants were expressed at a comparable level to that of the WT cells (***Figure 18***). Untransfected HEK-M1 cells were kept as a negative control, which showed no mCherry::Nir2 expression (since the mCherry-specific primary antibody was used to probe for the overexpressed protein and thus, we did not pick up the endogenous Nir2 expression).

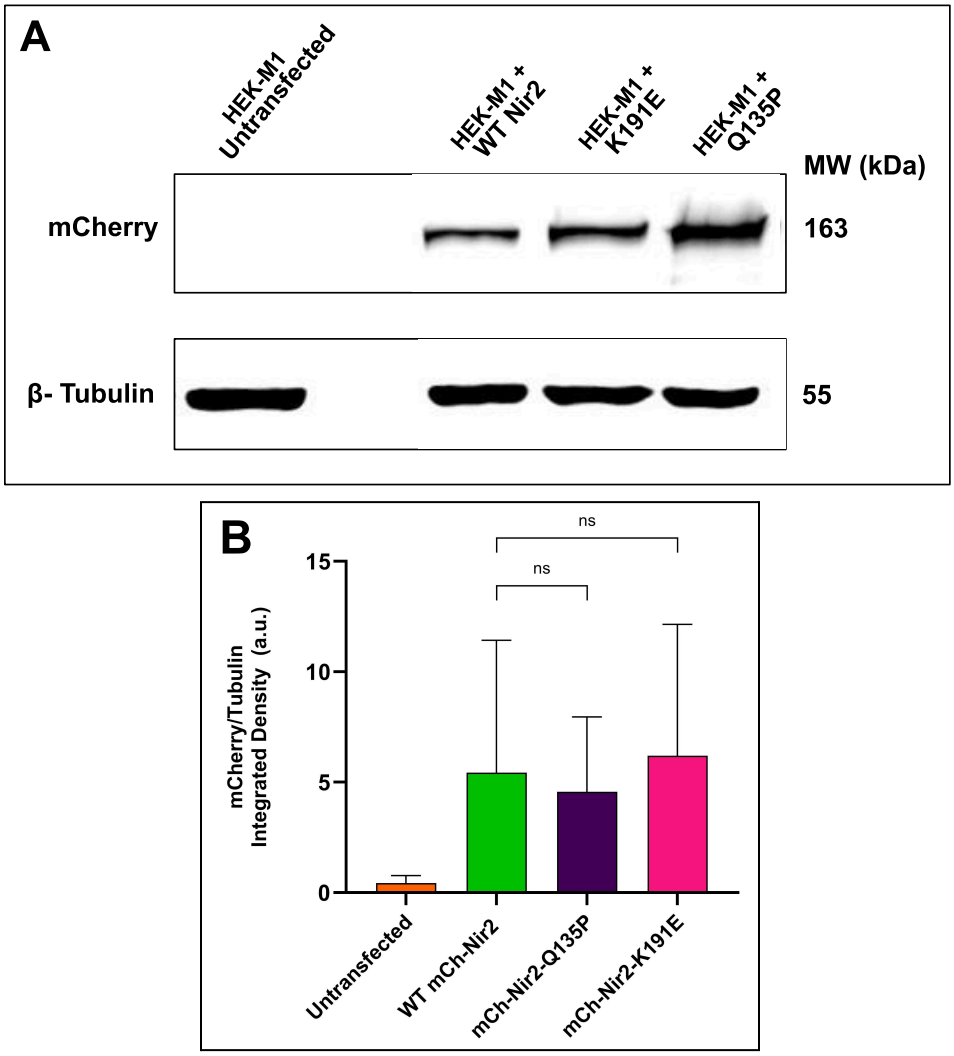


***Figure 18: Comparison of protein expression***
*Western Blot analysis showed both Q135P and K191E variants had similar expression levels as WT (B) Quantification of the Western Blot [average of integrated densities from 3 biological replicates, all values were normalised to tubulin; statistical test - Student's unpaired t test]*

## 6. Calcium Imaging Results Reveal that SNPs in the PITP Domain Affect Nir2 Function

Since the expression and localisation of both the variants (having either K191E or Q135P SNPs) were comparable to the WT cells, we hypothesised that there could be a functional defect that the SNPs might be causing, which could thereby translate into pathogenic effects. To test this hypothesis, we employed PLC-dependent intracellular $Ca^{2+}$ release as a physiological assay.

In our reporter HEK-M1 cell line, G-Protein Coupled Receptors (GPCRs) like m1AchR, when stimulated by specific agonists, activate Phospholipase C (PLC) that leads to the hydrolysis of Phosphatidylinositol 4, 5-bisphosphate ($PIP_2$) and generation of two second messengers, Diacylglycerol (DAG) and Inositol 1,4,5- trisphosphate ($IP_3$). $IP_3$ further binds to the $IP_3$ Receptor ($IP_3R$) present on the Endoplasmic Reticulum (ER), thereby activating them and facilitating the release of $Ca^{2+}$ from the ER stores.

Since Nir2 plays an important role in transferring PI to the plasma membrane, perturbation in the Nir2 function could affect the replenishment of the $PIP_2$ pool at the plasma membrane. This, in turn, could affect the downstream signalling, ultimately perturbing the intracellular $Ca^{2+}$ release. We used a ratiometric cytoplasmic $Ca^{2+}$ dye Fura-2 AM to measure the agonist [Carbamoylcholine chloride (Cch)] mediated intracellular $Ca^{2+}$ ($[Ca2+]_i$) release as a functional readout for Nir2.

We validated our assay by comparing $[Ca^{2+}]_i$ in HEK-M1-Nir2 shRNA cells (Nir2 depleted cells) and the HEK-M1-Scrambled shRNA cells (Control cells). We observed that upon activation with Cch, Nir2-depleted cells had a decreased rise in $[Ca^{2+}]_i$, compared to the control cells (***Figure 19A***). It is important to note that the basal $[Ca^{2+}]_i$ levels were in a similar range for both cell types (***Figure 19B***).

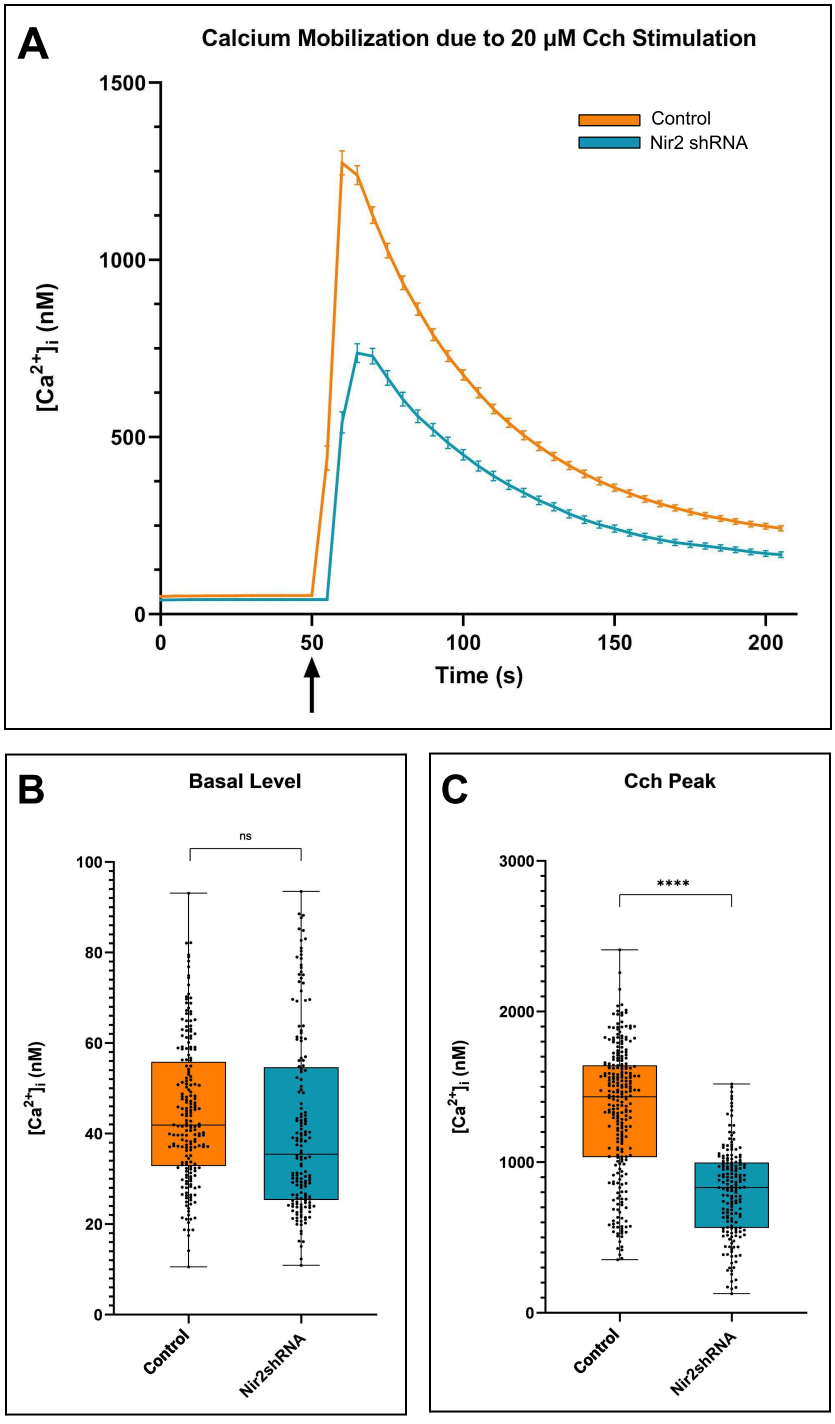


***Figure 19: $[Ca^{2+}]_i$ in Control and Nir2 depleted HEK-M1 cells***

*(A) Agonist (Cch) dependent calcium mobilisation was decreased in Nir2 depleted HEK-M1 cells, compared to the control cells. (B) Basal $[Ca^{2+}]i$ was unchanged. (C) Maximum $[Ca^{2+}]i$ observed was higher for control cells. [ n= ~120 for both; performed 5 replicates; statistical test - Student's unpaired t-test (p value < 0.0001)]*

After confirming that the assay was functional, we wanted to test whether cells independently transfected with WT mCherry::Nir2 plasmid could rescue the decreased $[Ca^{2+}]_i$, observed in the HEK-M1-Nir2 shRNA cells.

Thus, we overexpressed WT mCherry::Nir2 in the background of Nir2 depleted cells to check whether these cells were able to rescue the decreased $Ca^{2+}$ release phenotype shown by the Nir2 depleted cells.

For accurate measurements of $[Ca^{2+}]_i$, cells having both Fura 2-AM and mCherry signal were picked for the analysis (***Figure 20***).

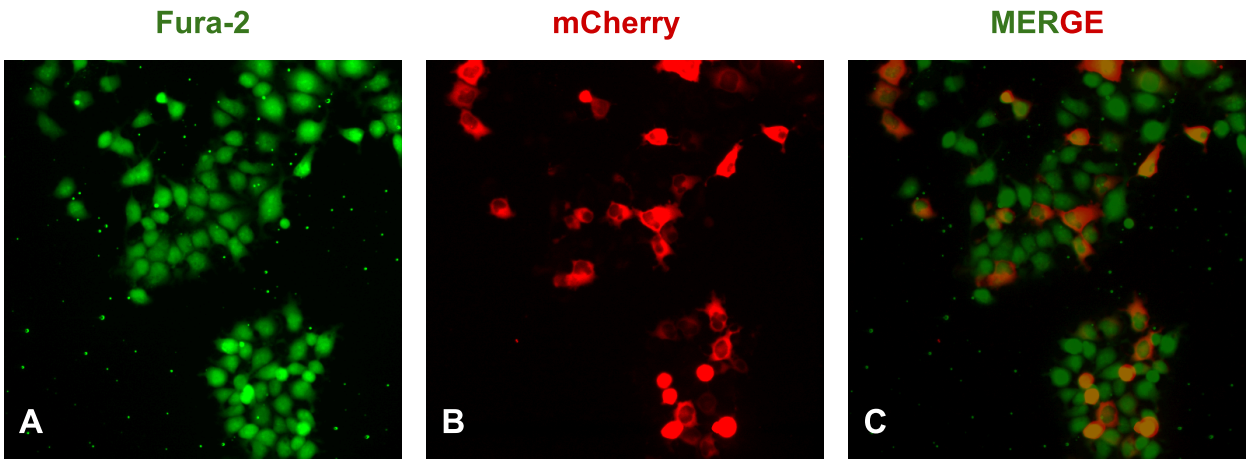


***Figure 20: Selection of HEK-M1 cells to be used for analysis***
*(A) All the cells stained with Fura 2-AM dye (B) Cells transfected with mCherry::Nir2 construct (C) Cells showing both Fura 2-AM and mCherry fluorescence picked for quantification of* $[Ca^{2+}]_i$

We observed that the decreased $[Ca^{2+}]_i$ in Nir2 depleted cells was successfully rescued by overexpressing mCherry::Nir2 in the background of Nir2 depleted cells (***Figure 21***). Similar to before, the basal $[Ca^{2+}]_i$ levels were in the similar range for all the cells.

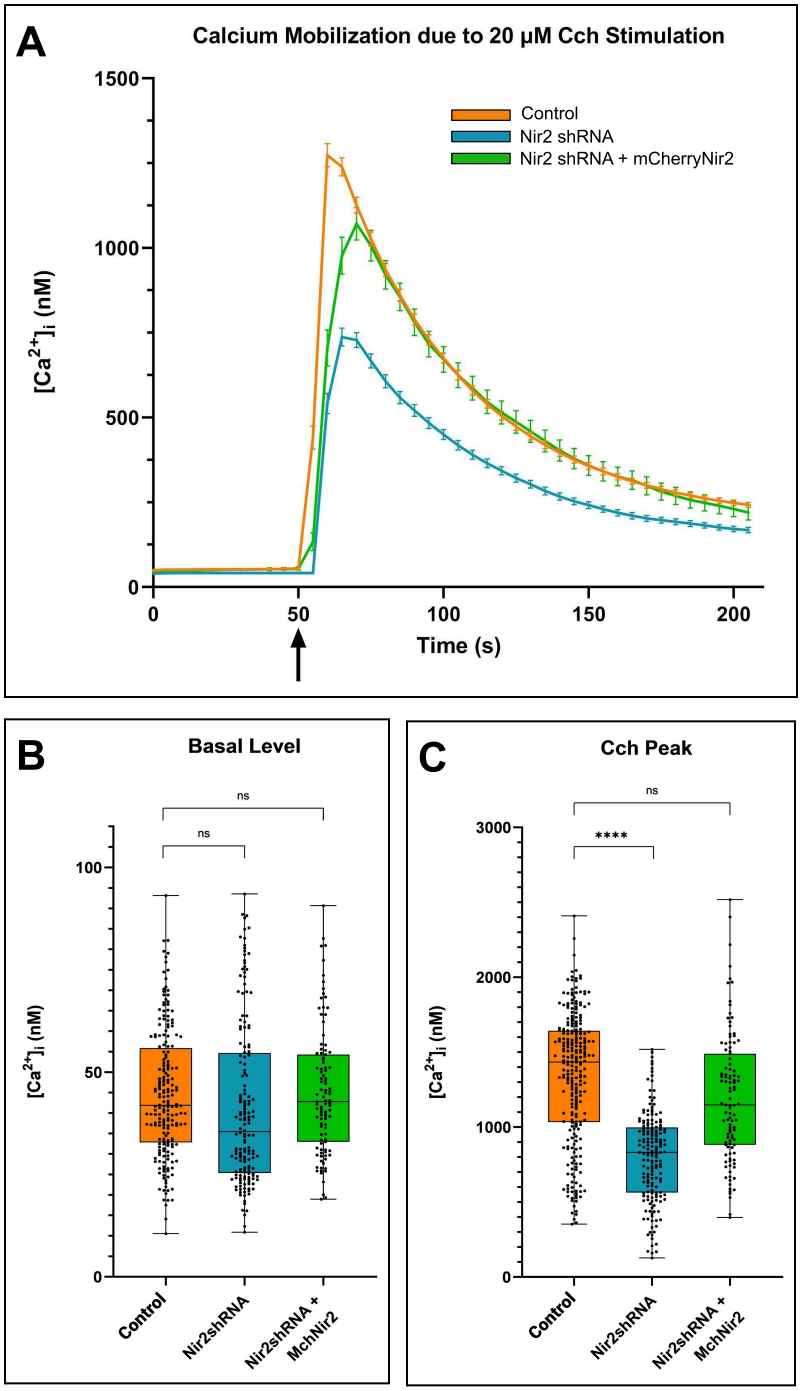


***Figure 21: Rescue of decreased $[Ca^{2+}]_i$ of Nir2 depleted HEK-M1 cells***

*(A) Overexpression of WT mCherry::Nir2 in the background of Nir2 depleted HEK-M1 cells rescued the decreased calcium mobilisation phenotype. (B) Basal $[Ca^{2+}]_i$ was unchanged (C) Maximum $[Ca^{2+}]_i$ observed was comparable for control and WT-Rescue cells. [ n= ~120 for all data sets; performed 5 replicates; statistical test - one-way ANOVA]*

Once our assay was established, we overexpressed Nir2 constructs having either of the SNPs in Nir2 depleted cells to investigate whether these cells were able to rescue the decreased $Ca^{2+}$ release phenotype, observed in the Nir2 depleted cells. We observed that both Nir2 variants were unable to rescue the decreased $[Ca^{2+}]_i$, confirming our hypothesis that SNPs in the PITP domain of Nir2 were affecting the protein's function (***Figure 22***).

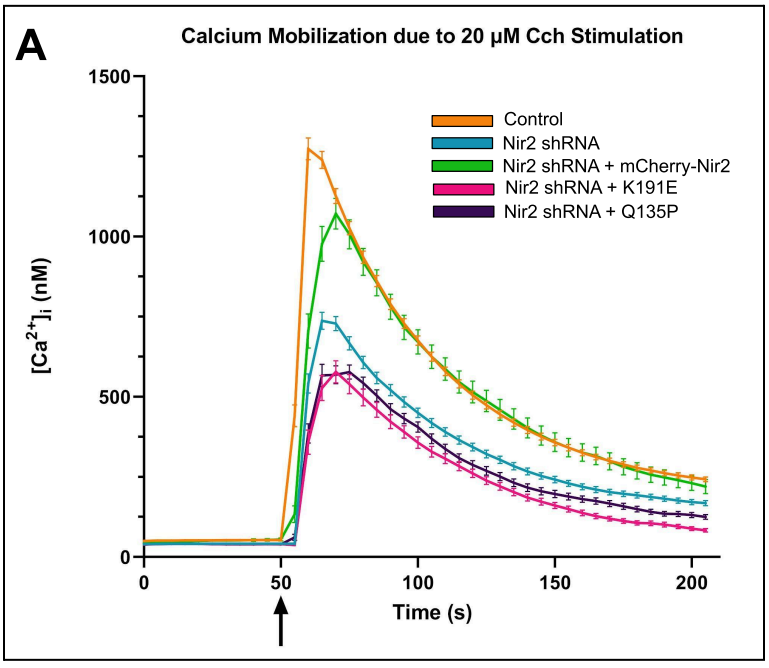


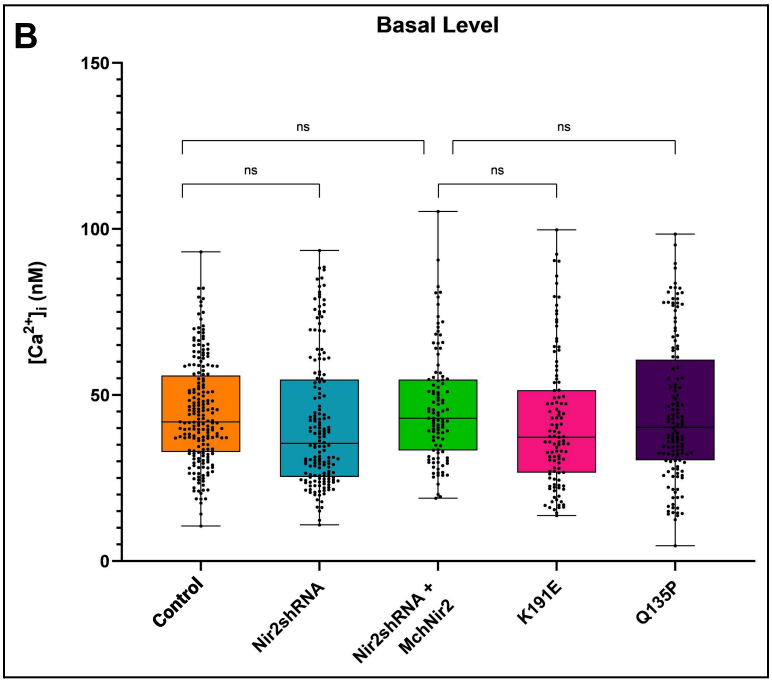

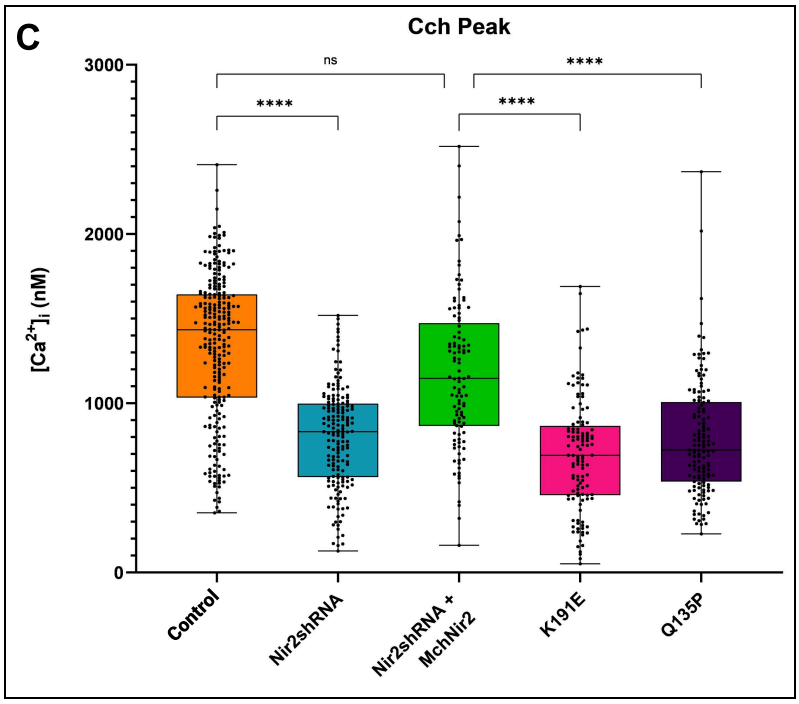


***Figure 22: $[Ca^{2+}]_i$ in Nir2 variant HEK-M1 cells***

*(A) Both Q135P and K191E variant HEK-M1 cells have decreased calcium mobilisation, compared to the rescue (B) Basal $[Ca^{2+}]_i$ was unchanged (C) Maximum $[Ca^{2+}]_i$ observed was significantly decreased, compared to the rescue. [ n= ~120 for all data sets; performed 5 replicates; statistical test - one way ANOVA]*

## CHAPTER V: DISCUSSION

Nir2 is a PITP that operates at the ER-PM contact sites to transfer PI and PA between membranes. The transfer of these molecules is essential to maintain the $PIP_2$ levels at the PM in a GPCR-mediated, PLC-activation pathway. $PIP_2$ is a critically important phosphoinositide that is a key regulator of a multitude of cellular processes, including intracellular $Ca^{2+}$ homeostasis. Thus, aberrant Nir2 function can lead to failure in replenishing the $PIP_2$ pool at PM, thereby leading to perturbed $Ca^{2+}$ homeostasis in cells. There is compelling evidence that perturbed $Ca^{2+}$ homeostasis in cells could be the causal mechanism behind the onset and progression of several neurodegenerative disorders, including Spinocerebellar Ataxia (SCA).

In this project, we aimed to evaluate the effect of non-synonymous SNPs in the PITP domain of Nir2, observed in patients showing clinical features like cerebellar dysfunction, suggestive of SCA.

Analysis using *in silico* tools showed that the amino acid residues under our study were conserved across PITPs. Thus, the substitutions caused by SNPs were predicted to be rare in nature and likely affect the protein's function. Molecular dynamics simulations run on a protein-membrane complex revealed that one of the SNPs (K191E) induces large movements between the protein and the membrane while also notably decreasing the protein's stability. Since Nir2 (and RDGB) is a contact-site protein, stable interaction with the membrane is an important readout for its functional properties. Thus, we infer from this that the amino acid substitution under study is predicted to affect the protein's function.

Experimental validation of these predictions, done in HEK 293T-M1 cells, showed no changes in the expression and localisation of the Nir2 variant proteins (Nir2-K191E and Nir2-Q135P) compared to the wild-type protein. However, there was a significant decrease of intracellular $Ca^{2+}$ release from the ER stores upon PLC-activation in both the Nir2 variant cells, compared to the wild-type cells. This indicates a functional

impairment in the Nir2 variants, as revealed by our assay, which serves as a readout of Nir2 function.

These results are in agreement with our hypothesis that SNPs in the PITP domain of Nir2 might contribute to the underlying mechanisms of cerebellar dysfunction by affecting the protein's function, and subsequently perturbing PLC-mediated $Ca^{2+}$ homeostasis in the cells. But how is the expression of these missense variations in the *PITPNM1* gene linked with the manifestation of the neurodegenerative phenotypes in patients? If the *PITPNM1* gene shows monoallelic expression, it is clear that the allele carrying the mutation could be getting expressed in the patients, potentially resulting in the clinical onset of neurodegenerative symptoms. However, if the gene shows biallelic expression, it is likely that the mutation is dominant-negative in nature (since the SNPs reported in patients were heterozygous). However, experiments need to be performed to assess the allelic expression of Nir2.

Moreover, since PLC-mediated $Ca^{2+}$ mobilisation indirectly correlates to the altered $PIP_2$ levels at the PM, it would be interesting to compare the rate of resynthesis of $PIP_2$ upon PLC activation in Nir2 variant cells with wild-type cells as a direct readout of Nir2 function. This can be addressed by employing imaging tools like a $PIP_2$-specific probe or by biochemical approaches like $PIP_2$ quantification using Liquid Chromatography with tandem mass spectrometry (LC-MS/MS). Although altered $PIP_2$ levels in Nir2 variants upon PLC activation can provide proof of functional impairment in Nir2 due to SNPs, it can not provide definitive insights into whether this impairment is primarily attributable to perturbations in the PI binding or PI transport mechanisms of the protein. Previous studies have identified crucial PI binding residues in PITPα and RDGB proteins. Mutating any of these residues results in the protein's inability to bind PI and support $IP_3$ generation *in vivo* (Tilley et al., 2004; Yadav et al., 2015). Notably, the SNPs under this study are positioned in close proximity (3.4 - 4.4 Å) to these conserved PI binding residues (***Figure 23***), suggesting their potential involvement in PI binding.

An immediate future direction involves placing the protein above a DPPC membrane substituted with 10% PI, and running molecular dynamics simulations on the complex to investigate any differential PI binding capabilities of variant proteins compared to the WT. To assess if the SNPs affect the protein's lipid-binding capability, lipid transfer assays, as detailed by Cockcroft S. (2009), can be conducted. Disruption of either of Nir2 functions- PI binding or transfer can further lead to depletion of the $PIP_2$ pool at the PM and the downstream $Ca^{2+}$ homeostasis.

The identification of SNPs within the *PITPNM1* gene as an underlying cause of neurodegeneration holds significant implications for understanding and managing the disorder. Early detection of such genetic variations can enable proactive monitoring and interventions, potentially delaying the onset of clinical symptoms. It can also help identify the risk of conceiving through genetic counselling in case a history of the mutation exists in the family.

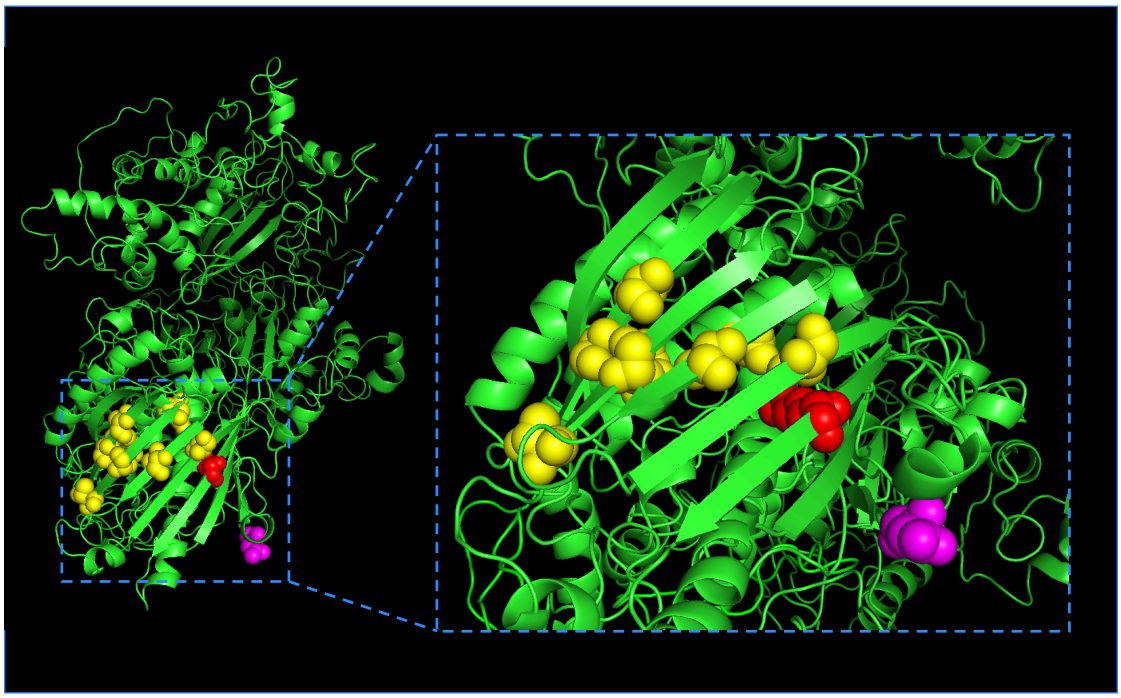

***Figure 23: RDGB Protein annotated with PI binding residues***
*The amino acid residues under study- K202 (red) and N135 (pink) are in close proximity to conserved PI binding residues (yellow).*

## References


1. Abe, S., Kobayashi, K., Oji, A., Sakuma, T., Kazuki, K., Takehara, S., Nakamura, K., Okada, A., Tsukazaki, Y., Senda, N., Honma, K., Yamamoto, T., Ikawa, M., Chiba, K., Oshimura, M., & Kazuki, Y. (2017). Modification of single-nucleotide polymorphism in a fully humanized CYP3A mouse by genome editing technology. *Scientific reports*, 7(1), 15189. https://doi.org/10.1038/s41598-017-15033-0

2. Adzhubei, I., Jordan, D. M., & Sunyaev, S. R. (2013). Predicting functional effect of human missense mutations using PolyPhen-2. Current protocols in human genetics, Chapter 7, Unit7.20. https://doi.org/10.1002/0471142905.hg0720s76

3. Amarilio, R., Ramachandran, S., Sabanay, H., & Lev, S. (2005). Differential regulation of endoplasmic reticulum structure through VAP-Nir protein interaction. *The Journal of biological chemistry*, *280*(7), 5934–5944. https://doi.org/10.1074/jbc.M409566200

4. Balla T. (2013). Phosphoinositides: tiny lipids with giant impact on cell regulation. *Physiological reviews*, *93*(3), 1019–1137. https://doi.org/10.1152/physrev.00028.2012

5. Basak, B., Krishnan, H., & Raghu, P. (2021). Interdomain interactions regulate the localization of a lipid transfer protein at ER-PM contact sites. *Biology open*, *10*(3), bio057422. https://doi.org/10.1242/bio.057422

6. Berridge M. J. (1984). Inositol trisphosphate and diacylglycerol as second messengers. *The Biochemical journal*, *220*(2), 345–360. https://doi.org/10.1042/bj2200345

7. Bill, C. A., & Vines, C. M. (2020). Phospholipase C. *Advances in experimental medicine and biology*, *1131*, 215–242. https://doi.org/10.1007/978-3-030-12457-1_9

8. Berendsen, H. J. C., van der Spoel, D., & van Drunen, R. (1995). GROMACS: A

message-passing parallel molecular dynamics implementation. Computer *Physics Communications*, 91(1-3), 43-56. https://doi.org/10.1016/0010-4655(95)00042-e

9. Chang, C. L., Hsieh, T. S., Yang, T. T., Rothberg, K. G., Azizoglu, D. B., Volk, E., Liao, J. C., & Liou, J. (2013). Feedback regulation of receptor-induced Ca2+ signaling mediated by E-Syt1 and Nir2 at endoplasmic reticulum-plasma membrane junctions. *Cell reports*, *5*(3), 813–825. https://doi.org/10.1016/j.celrep.2013.09.038

10. Cockcroft, S., & Carvou, N. (2007). Biochemical and biological functions of class I phosphatidylinositol transfer proteins. *Biochimica et biophysica acta*, *1771*(6), 677–691. https://doi.org/10.1016/j.bbalip.2007.03.009

11. Cockcroft S. (2009). Measurement of phosphatidylinositol and phosphatidylcholine binding and transfer activity of the lipid transport protein PITP. Methods in molecular biology (Clifton, N.J.), 462, 363–377. https://doi.org/10.1007/978-1-60327-115-8_23

12. Dash, R., Munni, Y. A., Mitra, S., Choi, H. J., Jahan, S. I., Chowdhury, A., Jang, T. J., & Moon, I. S. (2022). Dynamic insights into the effects of nonsynonymous polymorphisms (nsSNPs) on loss of TREM2 function. *Scientific reports*, *12*(1), 9378. https://doi.org/10.1038/s41598-022-13120-5

13. Durr A. (2010). Autosomal dominant cerebellar ataxias: polyglutamine expansions and beyond. *The Lancet. Neurology*, *9*(9), 885–894. https://doi.org/10.1016/S1474-4422(10)70183-6

14. Fu, L., Niu, B., Zhu, Z., Wu, S., & Li, W. (2012). CD-HIT: accelerated for clustering the next-generation sequencing data. *Bioinformatics (Oxford, England)*, *28*(23), 3150−3152. https://doi.org/10.1093/bioinformatics/bts565

15. Hisatsune, C., Hamada, K., & Mikoshiba, K. (2018). $Ca^{2+}$ signalling and spinocerebellar ataxia. *Biochimica et biophysica acta. Molecular cell research*, *1865*(11 Pt B), 1733–1744. https://doi.org/10.1016/j.bbamcr.2018.05.009

16. Huang, L., Chardon, J. W., Carter, M. T., Friend, K. L., Dudding, T. E., Schwartzentruber, J., Zou, R., Schofield, P. W., Douglas, S., Bulman, D. E., & Boycott, K. M. (2012). Missense mutations in ITPR1 cause autosomal dominant congenital nonprogressive spinocerebellar ataxia. *Orphanet journal of rare diseases*, *7*, 67. https://doi.org/10.1186/1750-1172-7-67

17. Hsuan, J., & Cockcroft, S. (2001). The PITP family of phosphatidylinositol transfer proteins. Genome biology, 2(9), REVIEWS3011. https://doi.org/10.1186/gb-2001-2-9-reviews3011

18. Kasumu, A., & Bezprozvanny, I. (2012). Deranged calcium signalling in Purkinje cells and pathogenesis in spinocerebellar ataxia 2 (SCA2) and other ataxias. *Cerebellum (London, England)*, *11*(3), 630–639. https://doi.org/10.1007/s12311-010-0182-9

19. Kim, S., Kedan, A., Marom, M., Gavert, N., Keinan, O., Selitrennik, M., Laufman, O., & Lev, S. (2013). The phosphatidylinositol-transfer protein Nir2 binds phosphatidic acid and positively regulates phosphoinositide signalling. *EMBO reports*, *14*(10), 891–899. https://doi.org/10.1038/embor.2013.113

20. Kim, Y. J., Guzman-Hernandez, M. L., Wisniewski, E., & Balla, T. (2015). Phosphatidylinositol-Phosphatidic Acid Exchange by Nir2 at ER-PM Contact Sites Maintains Phosphoinositide Signaling Competence. *Developmental cell*, *33*(5), 549–561. https://doi.org/10.1016/j.devcel.2015.04.028

21. Kim, Y. J., Guzman-Hernandez, M. L., Wisniewski, E., Echeverria, N., & Balla, T. (2016). Phosphatidylinositol and phosphatidic acid transport between the ER and plasma membrane during PLC activation requires the Nir2 protein. *Biochemical Society transactions*, *44*(1), 197–201. https://doi.org/10.1042/BST20150187

22. Klockgether, T., Mariotti, C., & Paulson, H. L. (2019). Spinocerebellar ataxia. *Nature reviews. Disease primers*, *5*(1), 24. https://doi.org/10.1038/s41572-019-0074-3

23. Krishnan, H., Basak, B., Nath, V. R., Mishra, S., & Raghu, P. (2023). Structural

organization of RDGB (retinal degeneration B), a multi-domain lipid transfer protein: a molecular modelling and simulation based approach. *Journal of biomolecular structure & dynamics*, *41*(22), 13368–13382. https://doi.org/10.1080/07391102.2023.2179545

24. Lev, S., Hernandez, J., Martinez, R., Chen, A., Plowman, G., & Schlessinger, J. (1999). Identification of a novel family of targets of PYK2 related to Drosophila retinal degeneration B (rdgB) protein. *Molecular and cellular biology*, *19*(3), 2278–2288. https://doi.org/10.1128/MCB.19.3.2278

25. Marambaud, P., Dreses-Werringloer, U., & Vingtdeux, V. (2009). Calcium signaling in neurodegeneration. *Molecular neurodegeneration*, *4*, 20. https://doi.org/10.1186/1750-1326-4-20

26. Mistry, J., Chuguransky, S., Williams, L., Qureshi, M., Salazar, G. A., Sonnhammer, E. L. L., Tosatto, S. C. E., Paladin, L., Raj, S., Richardson, L. J., Finn, R. D., & Bateman, A. (2021). Pfam: The protein families database in 2021. Nucleic acids research, 49(D1), D412–D419. https://doi.org/10.1093/nar/gkaa913

27. Ng, P. C., & Henikoff, S. (2003). SIFT: Predicting amino acid changes that affect protein function. Nucleic acids research, 31(13), 3812–3814. https://doi.org/10.1093/nar/gkg509

28. Novak, M. J., Sweeney, M. G., Li, A., Treacy, C., Chandrashekar, H. S., Giunti, P., Goold, R. G., Davis, M. B., Houlden, H., & Tabrizi, S. J. (2010). An ITPR1 gene deletion causes spinocerebellar ataxia 15/16: a genetic, clinical and radiological description. Movement disorders : official journal of the Movement Disorder Society, 25(13), 2176–2182. https://doi.org/10.1002/mds.23223

29. Peretti, D., Dahan, N., Shimoni, E., Hirschberg, K., & Lev, S. (2008). Coordinated lipid transfer between the endoplasmic reticulum and the Golgi complex requires the VAP proteins and is essential for Golgi-mediated transport. *Molecular biology of the cell*, *19*(9), 3871–3884. https://doi.org/10.1091/mbc.e08-05-0498

30. Prakriya, M., & Lewis, R. S. (2015). Store-Operated Calcium Channels.

*Physiological reviews*, *95*(4), 1383–1436. https://doi.org/10.1152/physrev.00020.2014

31. Prole, D. L., & Taylor, C. W. (2019). Structure and Function of $IP_3$ Receptors. *Cold Spring Harbor perspectives in biology*, *11*(4), a035063. https://doi.org/10.1101/cshperspect.a035063

32. Raghu, P., Basak, B., & Krishnan, H. (2021). Emerging perspectives on multidomain phosphatidylinositol transfer proteins. *Biochimica et biophysica acta. Molecular and cell biology of lipids*, *1866*(9), 158984. https://doi.org/10.1016/j.bbalip.2021.158984

33. Saha, S., Krishnan, H., & Raghu, P. (2023). IMPA1 dependent regulation of phosphatidylinositol 4,5-bisphosphate and calcium signalling by lithium. *Life science alliance*, *7*(2), e202302425. https://doi.org/10.26508/lsa.202302425

34. Seidel, K., Siswanto, S., Brunt, E. R., den Dunnen, W., Korf, H. W., & Rüb, U. (2012). Brain pathology of spinocerebellar ataxias. *Acta neuropathologica*, *124*(1), 1–21. https://doi.org/10.1007/s00401-012-1000-x

35. Shastry B. S. (2007). SNPs in disease gene mapping, medicinal drug development and evolution. *Journal of human genetics*, *52*(11), 871–880. https://doi.org/10.1007/s10038-007-0200-z

36. Sievers, F., Wilm, A., Dineen, D., Gibson, T. J., Karplus, K., Li, W., Lopez, R., McWilliam, H., Remmert, M., Söding, J., Thompson, J. D., & Higgins, D. G. (2011). Fast, scalable generation of high-quality protein multiple sequence alignments using Clustal Omega. Molecular systems biology, 7, 539. https://doi.org/10.1038/msb.2011.75

37. Slee, J. A., & Levine, T. P. (2019). Systematic prediction of FFAT motifs across eukaryotic proteomes identifies nucleolar and eisosome proteins with the predicted capacity to form bridges to the endoplasmic reticulum. Contact (Thousand Oaks (Ventura County, Calif.)), 2, 1–21. https://doi.org/10.1177/2515256419883136

38. Tilley, S. J., Skippen, A., Murray-Rust, J., Swigart, P. M., Stewart, A., Morgan, C. P., Cockcroft, S., & McDonald, N. Q. (2004). Structure-function analysis of human [corrected] phosphatidylinositol transfer protein alpha bound to phosphatidylinositol. Structure (London, England : 1993), 12(2), 317–326. https://doi.org/10.1016/j.str.2004.01.013

39. Trivedi, D., & Padinjat, R. (2007). RdgB proteins: functions in lipid homeostasis and signal transduction. *Biochimica et biophysica acta*, *1771*(6), 692–699. https://doi.org/10.1016/j.bbalip.2007.04.014

40. Van Durme, J., Delgado, J., Stricher, F., Serrano, L., Schymkowitz, J., & Rousseau, F. (2011). A graphical interface for the FoldX forcefield. Bioinformatics (Oxford, England), 27(12), 1711–1712. https://doi.org/10.1093/bioinformatics/btr254

41. Yadav, S., Garner, K., Georgiev, P., Li, M., Gomez-Espinosa, E., Panda, A., Mathre, S., Okkenhaug, H., Cockcroft, S., & Raghu, P. (2015). RDGBα, a PtdIns-PtdOH transfer protein, regulates G-protein-coupled PtdIns(4,5)P2 signalling during Drosophila phototransduction. *Journal of cell science*, *128*(17), 3330–3344. https://doi.org/10.1242/jcs.173476

42. Yates, C. M., & Sternberg, M. J. (2013). The effects of non-synonymous single nucleotide polymorphisms (nsSNPs) on protein-protein interactions. *Journal of molecular biology*, *425*(21), 3949–3963. https://doi.org/10.1016/j.jmb.2013.07.012

43. Zambonin, J. L., Bellomo, A., Ben-Pazi, H., Everman, D. B., Frazer, L. M., Geraghty, M. T., Harper, A. D., Jones, J. R., Kamien, B., Kernohan, K., Koenig, M. K., Lines, M., Palmer, E. E., Richardson, R., Segel, R., Tarnopolsky, M., Vanstone, J. R., Gibbons, M., Collins, A., Fogel, B. L., … Boycott, K. M. (2017). Spinocerebellar ataxia type 29 due to mutations in ITPR1: a case series and review of this emerging congenital ataxia. Orphanet journal of rare diseases, 12(1), 121. https://doi.org/10.1186/s13023-017-0672-7

44. Zündorf, G., & Reiser, G. (2011). Calcium dysregulation and homeostasis of neural calcium in the molecular mechanisms of neurodegenerative diseases provide multiple targets for neuroprotection. *Antioxidants & redox signalling*, *14*(7), 1275–1288. https://doi.org/10.1089/ars.2010.3359